



Contents lists available at ScienceDirect

European Journal of Medicinal Chemistry

journal homepage: <http://www.elsevier.com/locate/ejmech>

Research paper

## Discovery of indazole-pyridinone derivatives as a novel class of potent and selective MNK1/2 kinase inhibitors that protecting against endotoxin-induced septic shock

Agnieszka Dreas<sup>a,\*</sup>, Katarzyna Kucwaj-Brysz<sup>a</sup>, Karolina Pyziak<sup>a</sup>, Urszula Kulesza<sup>a</sup>, Ewelina Wincza<sup>b</sup>, Charles-Henry Fabritius<sup>a</sup>, Kinga Michalik<sup>a</sup>, Ewelina Gabor-Worwa<sup>a</sup>, Anieli Gołas<sup>a</sup>, Mariusz Milik<sup>a</sup>, Magdalena Masiejczyk<sup>a</sup>, Eliza Majewska<sup>a</sup>, Kazimiera Pyśniak<sup>c</sup>, Urszula Wójcik-Trechcińska<sup>c</sup>, Zuzanna Sandowska-Markiewicz<sup>c</sup>, Krzysztof Brzózka<sup>a</sup>, Jerzy Ostrowski<sup>c,d</sup>, Tomasz Rzymyski<sup>a</sup>, Michal Mikula<sup>c,\*\*</sup>

<sup>a</sup> Ryvu Therapeutics S.A., H. L. Sternbacha 2, 30-394, Kraków, Poland<sup>b</sup> Selvita S.A., Bobrzyńskiego 14, 30-348, Kraków, Poland<sup>c</sup> Department of Genetics, Maria Skłodowska-Curie National Research Institute of Oncology, 02-781, Warsaw, Poland<sup>d</sup> Department of Gastroenterology, Hepatology and Clinical Oncology, Centre of Postgraduate Medical Education, 02-781, Warsaw, Poland

## ARTICLE INFO

## Article history:

Received 11 September 2020

Received in revised form

25 November 2020

Accepted 26 November 2020

Available online xxx

## Keywords:

MNK1/2 kinases

Kinase inhibitors

Sepsis

Inflammatory diseases

## ABSTRACT

The mitogen-activated protein kinase (MAPK)-interacting kinases 1 and 2 (MNKs 1/2) and their downstream target eIF4E, play a role in oncogenic transformation, progression and metastasis. These results provided rationale for development of first MNKs inhibitors, currently in clinical trials for cancer treatment. Inhibitors of the MNKs/eIF4E pathway are also proposed as treatment strategy for inflammatory conditions. Here we present results of optimization of indazole-pyridinone derived MNK1/2 inhibitors among which compounds **24** and **26**, selective and metabolically stable derivatives. Both compounds decreased levels of eIF4E Ser206 phosphorylation (pSer209-eIF4E) in MOLM16 cell line. When administered in mice compounds **24** and **26** significantly improved survival rates of animals in the endotoxin lethal dose challenge model, with concomitant reduction of proinflammatory cytokine levels – TNF $\alpha$  and IL-6 in serum. Identified MNK1/2 inhibitors represent a novel class of immunomodulatory compounds with a potential for the treatment of inflammatory diseases including sepsis.

© 2020 Elsevier Masson SAS. All rights reserved.

## 1. Introduction

The mitogen-activated protein kinase (MAPK) interacting protein kinases 1 and 2 (MNK1 and MNK2) have been extensively studied in the scope of their contribution to the development and progression of solid tumors and hematological malignancies [1–6].

**Abbreviations:** ADME, absorption, distribution, metabolism, and excretion; Boc, *tert*-butoxycarbonyl protecting group; DIPEA, diisopropylethylamine; DMF, dimethylformamide; DMSO, dimethyl sulfoxide; EtOAc, ethyl acetate; LPS, Lipopolysaccharide; NEt<sub>3</sub>, triethylamine; rt, room temperature; SAR, structure-activity relationship; TFA, trifluoroacetic acid; TLC, thin layer chromatography; WB, Western blot; XPhos, 2-dicyclohexylphosphino-2',4',6'-triisopropylbiphenyl.

\* Corresponding author.

\*\* Corresponding author.

*E-mail addresses:* [agnieszka.dreas@ryvu.com](mailto:agnieszka.dreas@ryvu.com) (A. Dreas), [michal.mikula@pib-nio.pl](mailto:michal.mikula@pib-nio.pl) (M. Mikula).

<https://doi.org/10.1016/j.ejmech.2020.113057>

0223-5234/© 2020 Elsevier Masson SAS. All rights reserved.

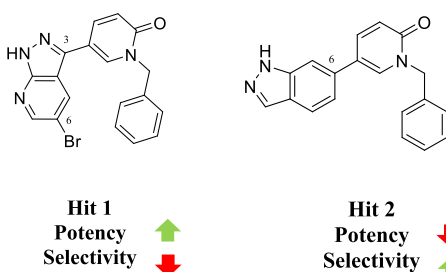
Established role in cancer and high druggability fueled development of first inhibitors [7,8]. MNK1 and MNK2 share substantial similarity in their coding sequences and protein structures [9]. MNK1 and MNK2 transcripts are alternatively spliced, giving rise to two distinct isoforms, with MNK1a/MNK2a representing a full-length protein and MNK1b/MNK2b, lacking the short MAPK binding C-terminal domain [10–12]. MNKs are phosphorylated at the C-terminus [13] by either ERK or p38 mitogen-activated protein kinases [14], hence the MNK1b/2b isoform poorly responds to activation and exhibits a low basal activity. In its turn, MNK1a represents an inducible isoform characterized by low basal levels of expression [15], while MNK2a is highly constitutively expressed [12]. MNKs play important roles in controlling post-transcriptional gene expression through Ser209 phosphorylation of the eukaryotic translation initiation factor 4E (eIF4E) [12,15,16]. Study involving double KO of MNK1/2 in mice indicates that MNK kinases are the

only proteins able to phosphorylate eIF4E [17]. This observation marked eIF4E phosphorylation as a potential biomarker for MNK1/2 inhibition studies. Recently, a number of studies suggested that eIF4E preferentially enhances the translation of mRNA coding tumor-associated proteins [18]. However, the control of 5'Cap-dependent translation may not be the sole function of MNK kinases. Additionally, these kinases demonstrate an ability to influence mRNA stability of TNF $\alpha$  or IL6, therefore playing an important role in modulating immune responses *via* mediation of cytokine production [19,20]. This pose an interesting avenue in the research, as TNF $\alpha$  is an important mediator of chronic and acute inflammation, including septic shock [21,22]. Sepsis is one of major health problems affecting millions of individuals world-wide each year. It ranks among the most common causes of death in hospitalized patients and represents a major healthcare financial burden world-wide [23]. Despite intense research efforts and clinical trials no specific treatment has been developed for this syndrome so far [24]. Several oncogenic and immune signaling pathways including PI3K/mTOR, RAS, ERK/p38-MAPK and Toll-like receptors pathways converge at the MNK kinases node to integrate signals into the initiation of translation and regulation of vital downstream processes of tumor cell biology and immune system [25]. As the MNKs are the only so far established kinases that activate oncogenic eIF4E this gave the rationale to develop nontoxic chemical inhibitors targeting these kinases for cancer treatment with possible reposition to treat autoimmune and inflammatory disorders, including sepsis. A large number of studies utilizing transient MNKs knockdown or pharmacological inhibition provided evidence on important MNK's role in mediating the production of multiple pro-inflammatory cytokines [8,19,26,27]. These studies highlighted importance on MNKs kinase node in mediating signals critical for pro-inflammatory responses, therefore the development of MNKs specific inhibitors could be a novel therapeutic approach for the treatment of inflammatory diseases, including sepsis.

Although MNK1 and MNK2 kinases play critical roles in autoimmune disorders and malignancies, expression of these proteins is not essential for normal growth and homeostasis in mice [17,20,28,29]. This distinction between normal and pathogenic function makes the MNKs particularly interesting as potential drug targets, with a broad therapeutic window. First MNK1/2 inhibitors (e.g. CGP052088, CGP57380 and Cercosporamide) mainly served as probes for target validation due to their low selectivity and potency. Further development led to the discovery of more specific and potent inhibitory agents [30–33], and eventually three MNKs inhibitors, namely ETC-206 [34], eFT508 [7] and BAY1143269 (full structure is still undisclosed) [8] developed by Experimental Therapeutics Centre, Effector Therapeutics and Bayer AG, respectively, have entered clinical trials in oncology [1] (Fig. 1).

Herein, we present the optimization of low molecular weight dual MNK1/2 inhibitors, which resulted in identification of

**Table 1**  
Characterization of the first hits for the MNK1/2 kinases.



	Hit1	Hit2
MNK1 IC <sub>50</sub> [nM]	56	315
MNK2 IC <sub>50</sub> [nM]	12	75

compounds **24** and **26**, endowed with high *in vitro* target selectivity. Oral treatment with the compound **26** decreased serum levels of TNF $\alpha$  and IL-6, significantly extended survival and improved clinical symptoms in a mouse model of endotoxin induced sepsis. These data indicate that the compound **26** could be considered for further development as an effective treatment of inflammatory diseases.

## 2. Results and discussion

### 2.1. Hit identification

First hits targeting MNK1/2 kinases were identified by the screening of the internal library of compounds using balanced reaction conditions for both kinases at  $K_m$  ATP concentration and ADP-Glo™ bioluminescent detection assay. As shown in Table 1, two hit compounds **1** and **2** were identified, sharing the same motif (pyridinone) in its structure. Hit **1** containing disubstituted (at positions C-3 – pyridinone and C-6 – bromine) aza-indazole core showed IC<sub>50</sub> of 56 and 12 nM for MNK1 and MNK2 kinases, respectively. The second chemotype had the same pyridinone moiety, however connected *via* the carbon atom at the C-6 position of an indazole core. Hit **2** showed IC<sub>50</sub> of 315 and 75 nM for MNK1 and MNK2 kinases, respectively.

Kinome selectivity of compounds **1** and **2** was tested at 1  $\mu$ M concentration by using KINOMEScan (DiscoverX) against 414 kinases. As demonstrated in Fig. 2A, hit **1** turned out as a multi-target compound, inhibiting significant number of kinases from panel. On the contrary, hit **2** showed excellent selectivity profile in the same panel with low selectivity score ( $S(35) = 0.01$ ). By using the <35% threshold of control activity (% Ctrl), only 3 kinases (except of

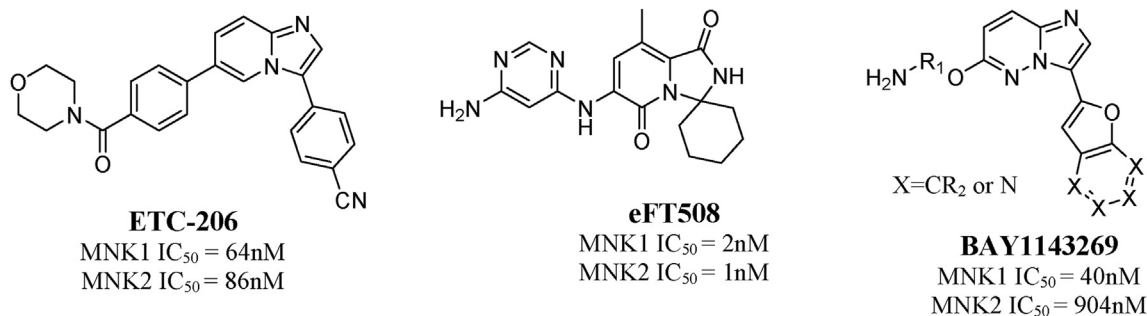


**Fig. 1.** Structures of MNKs inhibitors in clinical trials.

MNK2) were identified as hits (AAK1 32% Ctrl, ERK8 20% Ctrl and HASPIN 20% Ctrl). Those results prompted us to focus on further exploration of hit **2**.

## 2.2. Molecular studies

The structural aspects of MNK1 and MNK2 kinases were already broadly discussed in literature [1]. We may only emphasize here that despite the fact that they share the typical, two-domain, protein kinase architecture, the structures of MNKs contain several distinctive elements. The prominent characteristic is the replacement, of well conserved “DFG” sequence motif with “DFD” in the MNKs, which may influence both structural and functional aspects of their activity. Additionally, they are distinguished by the presence of the atypical sequence inclusions, including a Zn<sup>2+</sup> binding motif containing four cysteines, near the C terminus.

In order to rationally improve protein/ligand interactions, hit compounds were docked to known structures of MNK2 from Protein Data Bank (PDB) [35] using the Glide program from the Schrodinger Suite [36]. In the first approach, we docked compounds to the available active form structure of the MNK2 D228G mutant with staurosporine (PDB code: 2HW7) [37], however results were inconclusive, because of generally low values of docking scores and ambiguity of the protein/ligand interaction patterns. Poses of the compounds docked to this template were sometimes flipped by 180° in the MNK binding site, with no essential difference in the docking scores. One of the possible explanation was that the presence of high molecular weight staurosporine in the binding site caused substantial changes in the conformation of the binding site, amino acid side chains and some backbone atoms of amino acids from loops located in the vicinity of the ATP binding sites. Additionally, the combined effect of the D228G mutation and steric interactions of staurosporine ligand forced a conformational

change of the side chain of phenylalanine 227 in the 2HW7 complex. This new position was not entirely consistent with the conformation adopted by this residue in the native protein complexes.

In order to create an alternative version of the docking grid for MNK2, we used one of the apo structures of MNK2. At that time, there were two publicly available structures in PDB, namely 2AC3 and 2AC5. The former is a wild type, apo MNK2 in DFG/D-out conformation, the latter is a D228G mutant, apo MNK2 in DFG/D-in conformation. One of difficulties was that the binding sites of the kinase structures without ligand (apo) were too small to contain the ATP competitive ligand. Additionally, Phe227 in a DFG/D-out conformation was at the center positions of the ATP binding site. Induced Fit Docking (IFD) procedure, from the Schrodinger molecular modeling package removed small steric hindrances in the binding site. Changes introduced in the local conformation of the side chains and a flexible loop allowed docking of ligands to the protein model.

Selected representative active compounds were docked using the default IFD procedure from Protein Preparation Wizard [36]. The IFD-modified template on the basis of the MNK2 structure 2AC5 from PDB was selected given best docking score values and consistency of the docking poses. This model of MNK2 structure was used for SAR and evaluation rational ligand optimization. An example of such pose and analysis for hit compound **2** is presented in Fig. 3. In this pose, the main observed interaction is among atom 2-N from indazole moiety with Met162 residue in the hinge region of MNK2. Moreover, an important hydrogen bond interaction is created between a carbonyl group from pyridinone moiety and Lys113 residue.

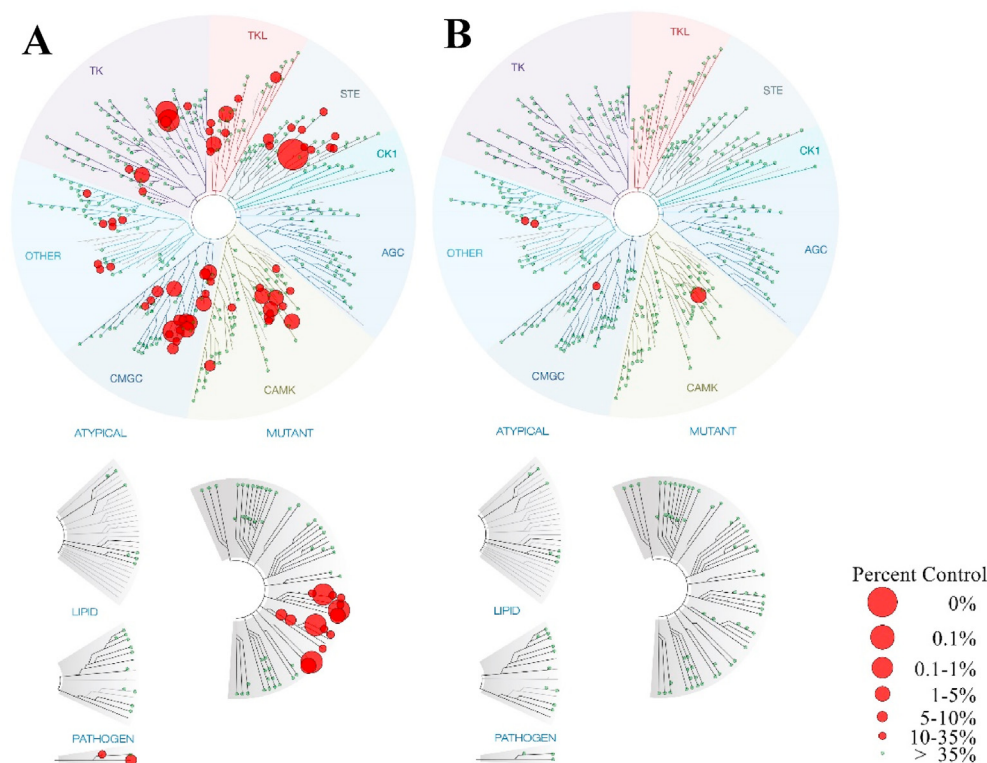


Fig. 2. Comparison of kinome selectivity panels for hit **1** (A) and hit **2** (B). Larger circle indicate higher affinity binding.

### 2.3. Chemistry

Although both hit compounds **1** & **2** were promising with respect to a potential optimization ( $LLE_{MNK2} = 4.8$  and  $LLE_{MNK2} = 4.3$  for hits **1** and **2**, respectively), our medicinal chemistry effort focused on the expansion of hit **2**. The first goal was to improve the potency by keeping high selectivity and good physicochemical/ADME properties. As shown in Fig. 4, the lead structure compound **1** was divided into two structural regions for hit optimization – the bicyclic core and the substitution on the pyridinone R.

The synthesis of the different bicyclic systems **1** to **5** is shown in Scheme 1. A Miyaura borylation reaction [38] of 1-benzyl-5-bromo-1,2-dihydropyridin-2-one [39] resulted in the formation of the boronic ester **29** (with additional boronic acid from 11% to 29%), which was subsequently coupled with 5-bromo-3-iodo-1-(triphenylmethyl)pyrazolo[3,4-*b*]pyridine [40] in Suzuki reaction to give compound **30** (Route A). Removal of the trityl protecting group from intermediate **30** in TFA conditions led to the hit **1** with moderate yield. Hit **2** (Route B) was synthesized using 1-benzyl-5-bromo-1,2-dihydropyridin-2-one and commercial 6-(4,4,5,5-tetramethyl-1,3,2-dioxaborolan-2-yl)-1*H*-indazole. Similarly, compounds **3**, **4** and **5** (Route C) have been obtained by coupling of boronic ester/acid **29** with the corresponding 6-bromoindole, 6-bromo-1-methyl-1*H*-indazole and 6-bromo-2-methyl-1*H*-indazole, respectively, with moderate yield.

The series of derivatives modified on the pyridinone (R-part – Fig. 4) have been synthesized in a similar way (Scheme 2). The appropriate boronic esters **32a-c**, prepared from *N*-substituted 5-bromopyridin-2(1*H*)-ones **31a,b,d** were reacted with 6-bromo-1*H*-indazole in the presence of  $PdCl_2(dppf) \cdot CH_2Cl_2$  to afford the final compounds **6**, **7** and **9**. *N*-acylation of 5-bromo-pyridin-2(1*H*)-one with 4-morpholine carbonyl chloride provided compound **31c** that was finally coupled with commercial 6-(4,4,5,5-tetramethyl-1,3,2-dioxaborolan-2-yl)-1*H*-indazole to give desired derivative **8** with moderate yield.

The series of derivatives bearing different substituents on benzyl ring (**10–28**) (Schemes 4 and 5) have been achieved by a

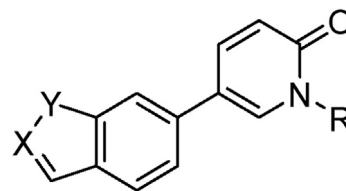


Fig. 4. General structure of compound I.

three-step synthesis starting from 5-bromopyridin-2(1*H*)-one, using the same type of reactions as described above. First, a set of different *N*-substituted 5-bromopyridin-2(1*H*)-one **33a-m** was prepared, as outlined on Scheme 3. Additionally, pyridinone **33m** was converted into the acetamide derivative **33n** using acetyl chloride/ $NEt_3$  in anhydrous  $CH_2Cl_2$  [41]. Few selected pyridinone derivatives with  $R_4 = H$  (**33a,b,d,g,h**) were transformed to the corresponding boronic esters (**34a-e**).

Suzuki coupling reactions between key intermediates **33a-l**, **33n** and 6-(tetramethyl-1,3,2-dioxaborolan-2-yl)-1*H*-indazole led to final compounds **10–17**, **20**, **22** and intermediates **35**, **36** and **37** as described in Scheme 4. Obtained intermediates **35** and **36** were converted into the final compounds **18** and **19** by basic hydrolysis of cyano group. Moreover, compound **21** was achieved from compound **37** by deprotection of Boc-group with a good yield.

The second group of compounds **23–28** was accomplished using the same type of coupling reaction between corresponding boronic esters/acid **29**, **34a-e** and 6-bromo-1*H*-indazol-3-amine with moderate to good yield (Scheme 5).

### 2.4. SAR study and ADME profiling

The first group of compounds **3–5** was synthesized to check the importance of the nitrogen atoms of the indazole core (Table 2). According to the docking studies, the nitrogen in position 2 creates an interaction with the hinge region. The replacement of the indazole moiety by an indole (compound **3**) resulted in the loss of biochemical potency as predicted. The same result was observed for the compounds **4** and **5** when the nitrogen atom in position 1 or 2, respectively, was methylated. Additional methyl group could change geometry of the compound in the binding pocket and impair essential interactions with the hinge region.

In order to increase the potency of hit compound **2**, we introduced modifications of the benzyl part (R substitution of the pyridinone (Fig. 4)). The incorporation of a longer, more flexible linker than methylene group (compound **6**) or the addition of a carbonyl group (compound **7**) resulted in inactive compounds (Table 3). The same result was obtained for compound **8** with a morpholine moiety. Finally, the complete removal of the aryl ring (compound **9**) resulted in the loss of potency as well, indicating the crucial role of the benzyl group for the activity of hit compound **2**. Further modifications of hit compound **2** involved decoration of the benzyl moiety.

Compounds **10–22** were synthesized with various substitutions on the aryl group as shown in Table 4. First, the effect of halogen atoms in different positions was examined. The fluorine atom (compound **10**) or chlorine atom (compound **12**) in *ortho* ( $R_2$ ) resulted in 2-fold activity improvement or the same level of activity, respectively, compared to hit compound **2** against MNK2. In case of MNK1 kinase, 7-fold activity improvement was observed for compound **10** and 4-fold for compound **12**, when compared to compound **2**. Substitutions in the *meta* position ( $R_3$ ) resulted also in the minor 2-fold improvement for both compounds **11** and **13** against MNK2. Notably, for MNK1 kinase, the tendency was

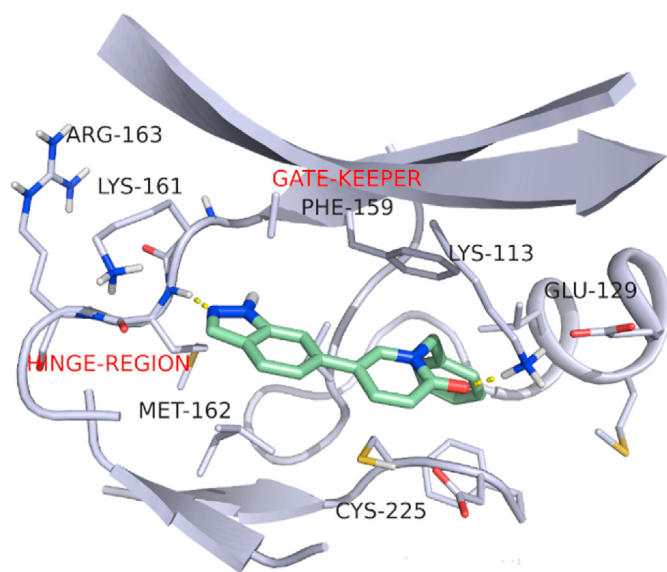
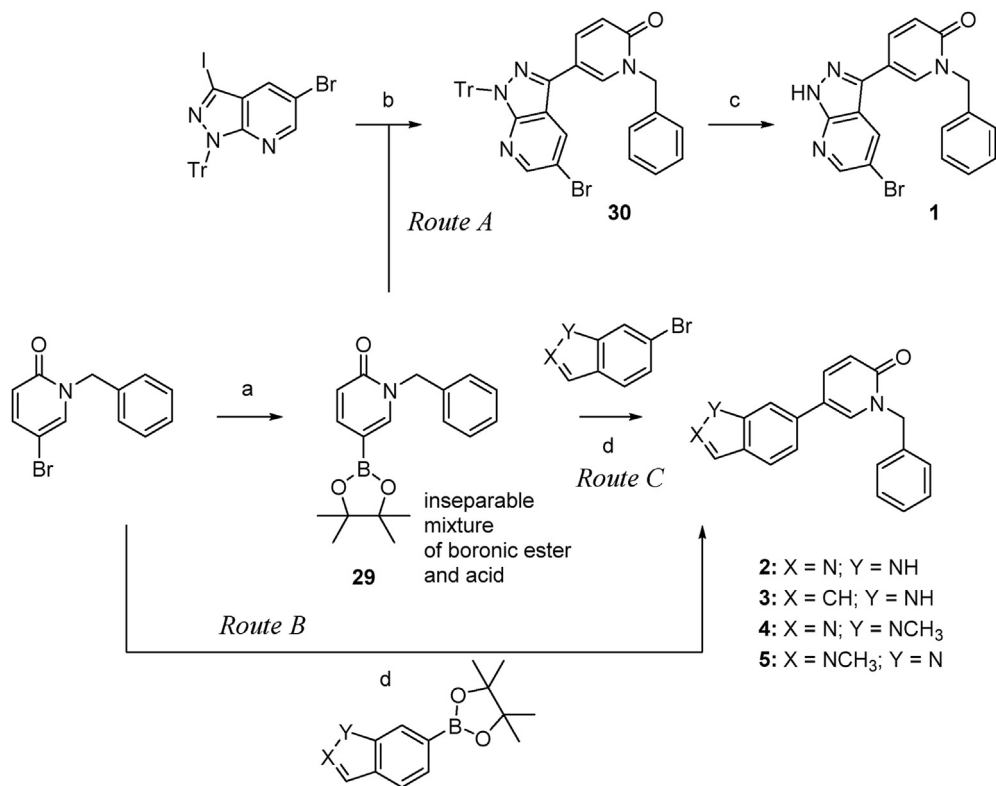
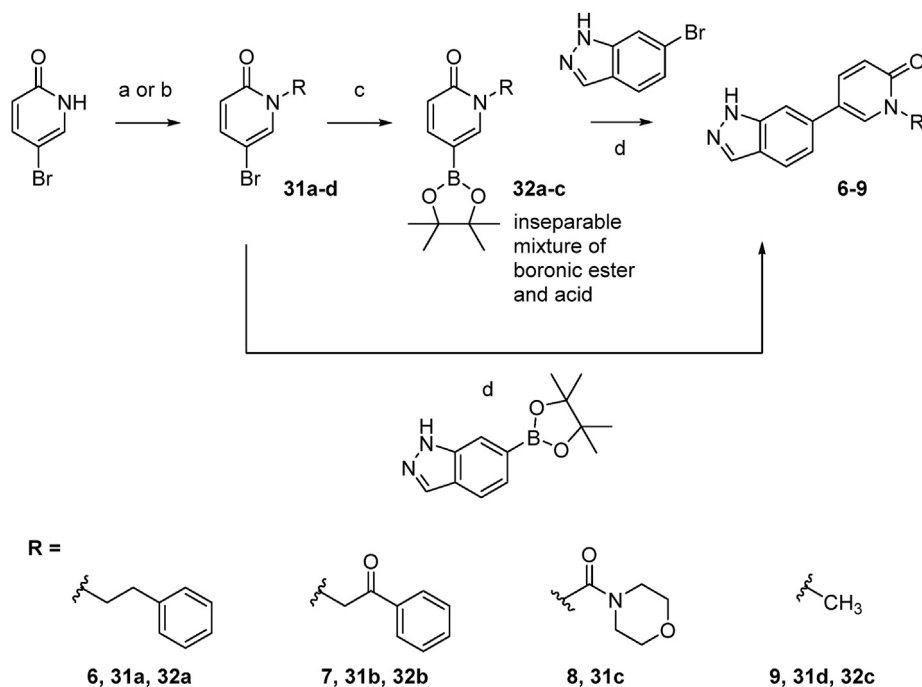


Fig. 3. Docking pose of compound “hit **2**” in MNK2 binding site, generated with use of Glide program (Schrodinger). The used template MNK2 structure was obtained by applying Induced Fit Docking procedure to the MNK2 structure 2AC5 from PDB, as it is described in text.



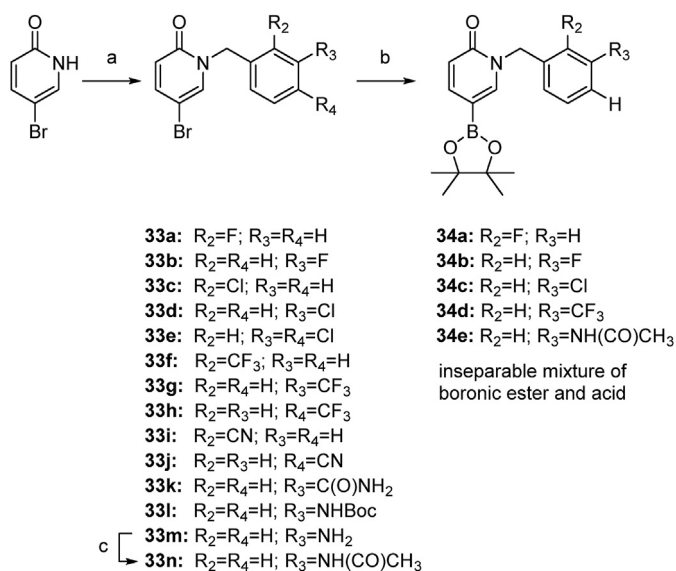
**Scheme 1.** Synthesis of bicyclic compounds **1–5**. Reagents and conditions: (a) bis(pinacolato)diboron, KOAc, XPhos, PdCl<sub>2</sub>(dppf)\*CH<sub>2</sub>Cl<sub>2</sub>, 1,4-dioxane, 100 °C; (b) sat. aq. sol. NaHCO<sub>3</sub>, PdCl<sub>2</sub>(dppf)\*CH<sub>2</sub>Cl<sub>2</sub>, acetonitrile/toluene (2/1), 60 °C, 50%; (c) TFA, CH<sub>2</sub>Cl<sub>2</sub>, rt, 64%; (d) Cs<sub>2</sub>CO<sub>3</sub>, PdCl<sub>2</sub>(dppf)\*CH<sub>2</sub>Cl<sub>2</sub>, 1,4-dioxane/water (2/1), microwave, 125 °C, 26–63%.



**Scheme 2.** Synthesis of compounds **6–9**. Reagents and conditions: (a) corresponding bromo- and iododerivatives, 60% NaH, DMF, 0 °C to rt, 12–95%; (b) 4-morpholine carbonyl chloride, DIPEA, acetonitrile, rt, 98%; (c) bis(pinacolato)diboron, KOAc, XPhos, PdCl<sub>2</sub>(dppf)\*CH<sub>2</sub>Cl<sub>2</sub>, 1,4-dioxane, 100 °C; (d) Cs<sub>2</sub>CO<sub>3</sub>, PdCl<sub>2</sub>(dppf)\*CH<sub>2</sub>Cl<sub>2</sub>, 1,4-dioxane/water (2/1), microwave, 125 °C, 32–53%.

opposite, with 4-fold increased activity of compound **11** with the fluorine atom and 8-fold improvement for compound **13** with the chlorine atom. The incorporation of two chlorine atoms in both

*meta* (R<sub>3</sub>) and *para* (R<sub>4</sub>) positions (compound **14**) led to a minor decrease in the activity against MNK2 kinase, however 5-fold increase for MNK1 kinase. These results prompted us to introduce



**Scheme 3.** Synthesis of intermediates **33a-n** and **34a-e**. Reagents and conditions: (a) corresponding benzyl bromide or chloride, 60% NaH, DMF, 0 °C to rt, 24–96%; (b) bis(pinacolato)diboron, KOAc, XPhos, PdCl<sub>2</sub>(dppf)·CH<sub>2</sub>Cl<sub>2</sub>, 1,4-dioxane, 100 °C; (c) acetyl chloride, NEt<sub>3</sub>, CH<sub>2</sub>Cl<sub>2</sub>, 0 °C to rt, 85%.

more bulky, electron-withdrawing groups, such as -CF<sub>3</sub>, as a possible alternative to the fluorine or chlorine atoms on the aryl group (compounds **15–17**). The most potent compound **16** contains a -CF<sub>3</sub> group in the *meta* position. Interestingly, compound **17** with the -CF<sub>3</sub> in *para* position turned out to be less active with a micromolar activity against both kinases. Compounds **18–20** with a polar amide group in *ortho*, *meta* and *para* position were less potent compared to hit compound **2**. Nevertheless, compounds **18–20**

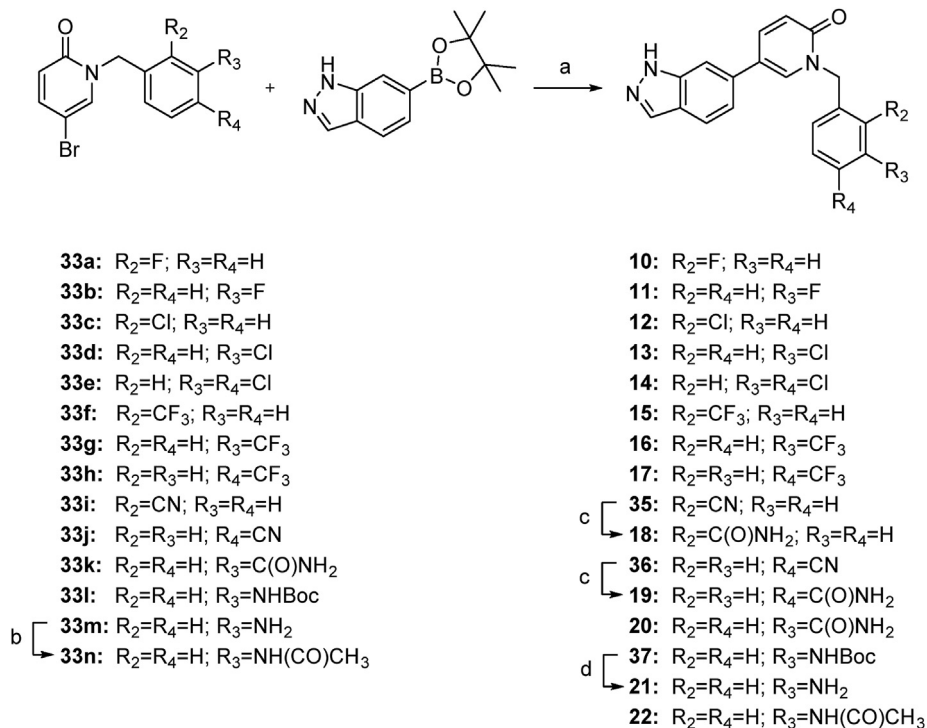
showed the same trend in increased activity – *meta* > *ortho* > *para*. Further exploration of the *meta* position with primary amine (compound **21**) and retro amide (compound **22**) resulted in either no improvement of potency or slightly, 2-fold, increase of the activity against both MNK1 and MNK2 kinase, respectively.

ADME profiling of hit compound **2**, revealed high microsomal clearance Cl<sub>int</sub> = 157 μl/min/mg (Table 5). Compounds **10 o-F**, **11 m-F** were also metabolically unstable (Mouse Cl<sub>int</sub> between 160 and 246 μl/min/mg), however compounds **13 m-Cl**, **16 m-CF<sub>3</sub>** and **22 m-NHCOCH<sub>3</sub>** showed moderate improvement in stability (Cl<sub>int</sub> between 47 and 63 μl/min/mg). As a potential strategy for further improvement of clearance applied overall reduction of lipophilicity in the current chemical series.

The introduction of a more polar group into the benzylic moiety resulted in an increase of the metabolic stability but disappointingly in a decrease of the biochemical activity on both MNK1 and MNK2. In order to improve the activity, a primary amine was introduced in the 3<sup>rd</sup> position of the indazole moiety to compounds **10**, **11**, **13**, **16**, **22** with the most promising decoration on the benzyl moiety (Table 6). This insertion resulted in compounds **23–28** showing a significant improvement of the metabolic stability in mouse microsomes (for most compounds Mouse Cl<sub>int</sub> < 10 μl/min/mg). At the same time, introduction of the amine moiety in the hinge region translated in an increase of the activity against MNK1/2 kinases for all compounds (improvement in potency from 1.5 to 9-fold for MNK2 and 3 to 4-fold for MNK1) compared to analogs without -NH<sub>2</sub> group.

Compounds with halogen substituents in benzylic moiety (**24 o-F** and **26 m-Cl**) were selected for further profiling given their high activity against MNK1/2 and low microsomal clearance Cl<sub>int</sub> < 10 μl/min/mg.

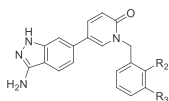
Notably, compounds **24** and **26** did not inhibit any tested CYP450 isoforms (IC<sub>50</sub> > 10 μM), showed high plasma protein binding and acceptable solubility (Table 7).



**Scheme 4.** Synthesis of compounds **10–22**. Reagents and conditions: (a) Cs<sub>2</sub>CO<sub>3</sub>, PdCl<sub>2</sub>(dppf)·CH<sub>2</sub>Cl<sub>2</sub>, 1,4-dioxane/water (2/1), microwave, 125 °C, 7–70%; (b) acetyl chloride, NEt<sub>3</sub>, CH<sub>2</sub>Cl<sub>2</sub>, 0 °C to rt, 85%; (c) K<sub>2</sub>CO<sub>3</sub>, 30% H<sub>2</sub>O<sub>2</sub>, MeOH/H<sub>2</sub>O (5/1), 0 °C to rt, 46–72%; (d) 4 M HCl in 1,4-dioxane, rt, 89%.



**Table 6**  
Improvement of potency and metabolic stability.



Compound	R <sub>2</sub>	R <sub>3</sub>	MNK2 IC <sub>50</sub> [nM]	MNK1 IC <sub>50</sub> [nM]	Cl <sub>int</sub> [μl/min/mg]
<b>23</b>	H	H	32	79	<10
<b>24</b>	F	H	4	12	<10
<b>25</b>	H	F	5	19	<10
<b>26</b>	H	Cl	6	11	<10
<b>27</b>	H	CF <sub>3</sub>	21	56	<10
<b>28</b>	H	NHCOCH <sub>3</sub>	8	55	14

**Table 7**  
ADME properties of compounds **24** and **26**.

Experiment		Compound 24	Compound 26
<b>CYP IC<sub>50</sub> [μM]</b>	3A4	>10	>10
	1A2	>10	>10
	2B6	>10	>10
	2C19	>10	>10
	2D6	>10	>10
<b>PPB</b>	mouse	93	90
	rat	>95	ND
	human	>95	ND
<b>Kinetic solubility [μM]</b>	Soerensen buffer	466	172
	water	>500	275

ND – not determined.

not affected by compound **24**. Low selectivity score ( $S(35) = 0.017$ ) indicate a small number of kinases that compound **24** interact with (ERK7 25% Ctrl, PASK 24% Ctrl, STK 17A 6% Ctrl, TBK1 35% Ctrl and TSF1 33% Ctrl). The second profiled compound **26** (Fig. 5B) displayed also very good selectivity ( $S(35) = 0.051$ ), confirming broad

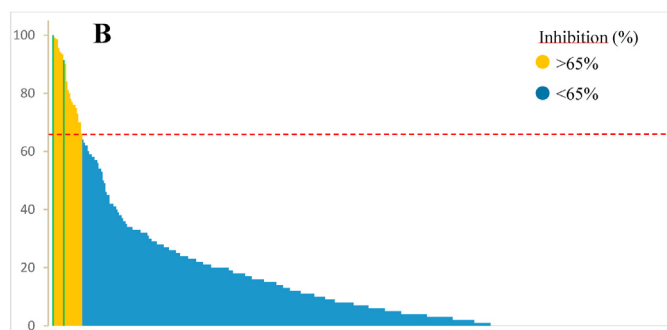
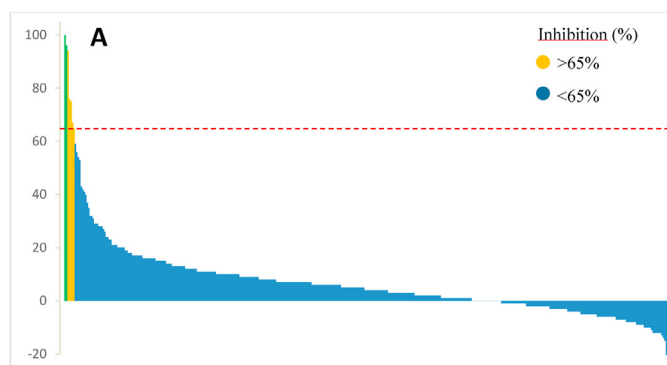


**Fig. 5.** Selectivity – kinome panel for compounds **24** (A) and **26** (B). (Inhibition = 100%-%Ctrl).

kinome selectivity. The off-targets were identified mostly from CMGC (CLK, DYRK, ERK, HIPK) and AGC (GRK and SGK) kinase family (Table 8).

## 2.6. Biochemical studies using recombinant MNK1 and MNK2

For better characterization of compounds **24** and **26**, the inhibition constant ( $K_i$ ) on MNK1 and MNK2 has been determined. The compounds were tested in the presence of increasing ATP concentrations:  $0.1 \times K_m$ ,  $0.3 \times K_m$ ,  $1 \times K_m$ ,  $3 \times K_m$ ,  $7 \times K_m$  of ATP for each kinase. IC<sub>50</sub> values for both compounds shifted over 3 times between  $0.3$  and  $7 \times K_m$  of ATP (data not shown), therefore competitive inhibition model has been applied to evaluate the inhibition constant (Fig. 6). For MNK1,  $K_i$  14 nM was measured for both compound **24** and **26**. For MNK2,  $K_i$  11 nM and 5.5 nM were measured for compound **24** and **26**, respectively.

## 2.7. Biological evaluation

Number of studies utilizing siRNA knockdown or small molecule inhibitors provided evidence on MNK's role in fine-tuning inflammatory and immune processes by influencing cytokines expression levels (reviewed in Ref. [20]). The first synthetic small-molecule MNK inhibitor, CGP57380, was shown to attenuate TNF $\alpha$  production in a dose-dependent manner in mice macrophages [42]. Subsequent studies using bone marrow-derived macrophages isolated from a mouse model of Crohn's disease and challenged with LPS revealed inhibition of the TNF $\alpha$ , IL6, MCP-1 and induction of IL10 levels by CGP57380 [19]. The work by Fortin et al. revealed that the CGP57380 attenuated production of several chemokines, including IL8, MIP-1-alpha and MIP-1-beta upon LPS- and TNF $\alpha$ -treatment, at

**Table 8**  
Activity of compound **26** towards selected off-target kinases.

Target	Kinase family	% Ctrl @1000 nM
<b>BIKE</b>	TK	1.2
<b>BMPR1B</b>	TKL	19
<b>CLK1</b>	CMGC	27
<b>CLK4</b>	CMGC	10
<b>DRAK1</b>	other	1.5
<b>ERK8</b>	CMGC	5.7
<b>FLT3</b>	mutant	22
<b>GRK4</b>	AGC	23
<b>HASPIN</b>	other	24
<b>HIPK4</b>	CMGC	30
<b>PIP5K2B</b>	lipid	24
<b>RIOK1</b>	atypical	34
<b>RIOK2</b>	atypical	6.2
<b>RIOK3</b>	atypical	4.4
<b>SGK</b>	AGC	30
<b>SGK3</b>	AGC	25

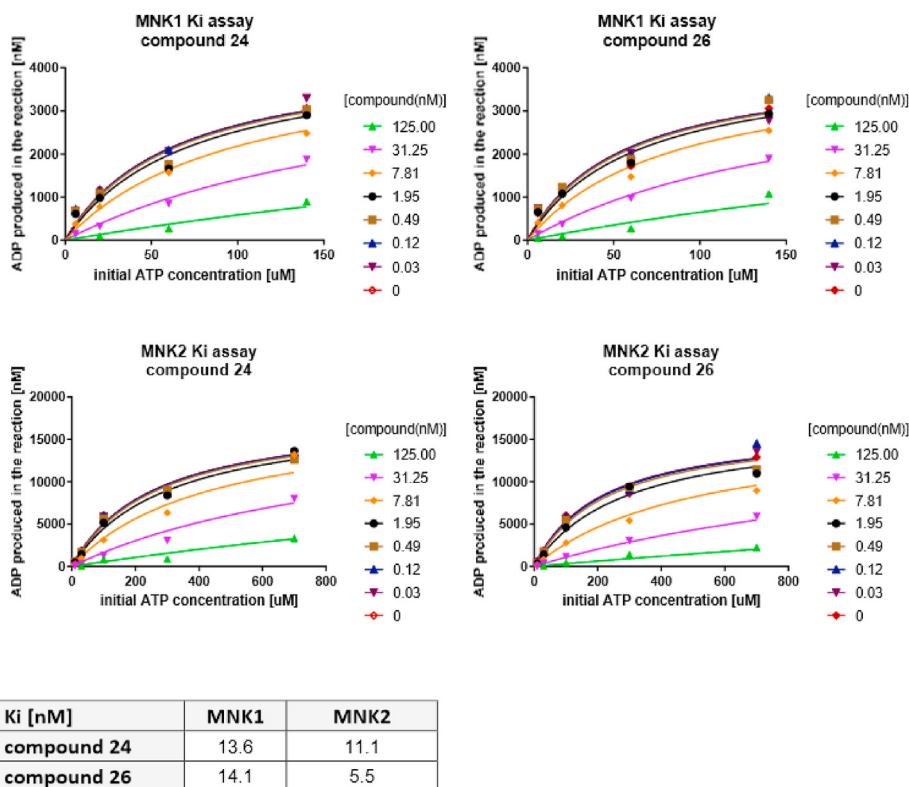


Fig. 6. The results from ATP competition test for compounds **24** and **26**.

the same time reversing the antiapoptotic effect of LPS and TNF $\alpha$  in human neutrophils [43]. More recently, the efficacy of another MNK kinase inhibitor, BAY1143269, was tested *ex vivo* on human whole blood challenged with LPS, revealing its potency to repress TNF $\alpha$ , IL6, MCP-1 and IL-1 $\beta$  pro-inflammatory cytokines production [8]. Collectively, these studies confirmed that pharmacological inhibition of MNK kinases can alter the cyto- and chemokines production in different immune cells, raising the possibility that selective targeting of MNK kinases may provide a potential novel therapeutic approach for the treatment of systemic inflammation, including sepsis.

### 2.7.1. *In vitro* studies

MNK kinases are the only proteins able to directly phosphorylate eIF4E at serine 209, what makes this modification a perfect biomarker for MNK1/2 inhibition studies. Cellular activity of compounds against MNK1/2 kinases could be conveniently tracked by measuring inhibitory effects in MOLM16 cell line characterized by a high basal levels of eIF4E Ser209 phosphorylation (pSer209-eIF4E).

Both compounds **24** and **26** showed dose and time-dependent inhibition of Ser209 without significant effects on total eIF4E levels (Fig. 7).

### 2.7.2. *In vivo* studies

Previous studies established MNK kinases as important regulators of pro-inflammatory cytokine production and cytokine signaling [20], therefore we tested if our compounds could have protective effects in mouse model of endotoxin-induced septic shock. *In vivo* mouse pharmacokinetics profile of both compounds **24** and **26** was determined after p.o. and i.v. dosing. The study revealed a relatively short half-life of both compounds in plasma and reached about 2 h (after p.o. administration) or 3 h (i.v.) for compound **24** and 1.8 h (p.o.) or 2 h (i.v.) for compound **26**. Nevertheless, both compounds showed oral bioavailability (33% and ~100% for compounds **24** and **26**, respectively). At  $T_{max}$  (0.25 h for both compounds) after p.o. administration, maximum plasma concentration for compound **26** was about 3-times higher than for compound **24** (1050 ng/ml versus 335 ng/ml, respectively).

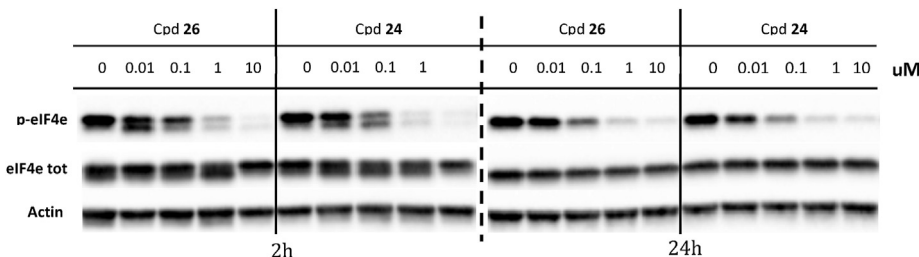


Fig. 7. Compounds **24** and **26** inhibit eIF4e phosphorylation in MOLM 16 cell line. MOLM16 cells were treated with indicated concentrations of compounds for 2h or 24h. Cell lysates were analyzed by immunoblotting with the eIF4E (C.sig.; 9741L), Phospho-eIF4E (Ser209) (C.sig.; 9742L) and b-Actin (Sigma; A2066) antibodies.

**Table 9**  
Pharmacokinetics parameters of compound **24** and **26** in mice (dose: p.o 5 mg/kg; i.v 2 mg/kg).

Compound	T <sub>max</sub> (h)	C <sub>max</sub> (ng/mL)	T <sub>1/2</sub> (h)	AUC <sub>0-t</sub> (ng/h·mL)	AUC <sub>0-∞</sub> (ng/h·mL)	F %
24 (p.o)	0.25	334.9	2.4	517.3	674.2	33
24 (i.v.)	0.08	1671.9	3.3	629.4	677.3	
26 (p.o)	0.25	1050.2	1.9	2149.2	2409.6	~100
26 (i.v.)	0.08	1493.1	2.1	833.9	855.4	

Difference in pharmacokinetics properties was also reflected in the plasma exposure, being 4-times higher for compound **26** than for compound **24** (Table 9). Based on these results, to assess efficacy of the compounds **24** and **26**, twice daily (BID) p.o. administration was proposed. Both compounds were well tolerated by the animals in long-term *in vivo* studies with BID p.o. dosing. Compound **26** was safe for the tumor-bearing mice at the dose of 50 mg/kg BID: general condition, body weight and blood clinical chemistry parameters were not affected during the 37-days treatment [3]. In the case of compound **24**, the dose of 100 mg/kg was administered p.o. with BID schedule to tumor-bearing mice for 17 consecutive days, and was well tolerated by the animals as assessed by the lack of clinical observations or body weight loss (data not shown).

The treatment of mice with either compound **24** or **26** probes before LPS lethal dose challenge followed by drugs administration BID significantly improved survival rates of animals (Fig. 8). Compound **24** and **26** treated groups exhibited significant recovery with ameliorated clinical symptoms including lethargy, hunched posture, and piloerection, compared with those in the LPS group alone. Given the protective effect of compounds on mice survival we next repeated experiment with 27 h endpoint following LPS challenge and surveyed levels of cytokines in serum. We found that compound **26**, but not **24**, significantly reduced level of pro-inflammatory TNF $\alpha$  and IL-6 (Fig. 9). A trend, but not significant, in abundances reduction was observed for other proteins including IL-22 and IL-1 $\beta$  with compound **26** treatment (data not shown). To the best of our knowledge this is the first study showing that pharmacological inhibition of MNKs as mediators of pro-inflammatory cytokine production exhibits highly protective effects and ameliorates clinical symptoms of the endotoxin induced sepsis.

### 3. Conclusions

In summary, a novel series of indazole-pyridinone derivatives

was developed as dual inhibitors of MNK1/2 kinases. Identified hit **2** proved to be moderately active against MNK1/2 kinases but selective in a kinome panel. Therefore, our goal was to improve potency while keeping high selectivity. Indeed, primary SAR analysis revealed that we managed to improve activity, however ADME profiling revealed high microsomal clearance of compounds. Decreasing overall lipophilicity by adding primary amine into the hinge region increase biochemical activity (19-fold for MNK2 and from 26-fold for MNK1 compared to hit **2**) and decreased hepatic clearance, without compromising overall favorable selectivity profile. *In vivo* studies using murine model of the endotoxin-induced sepsis indicated that selective MNK1/2 inhibitors are a novel promising class of compounds with a strong immunomodulatory activity and could be considered as candidate drugs for treatment of inflammatory syndromes including sepsis.

### 4. Experimental procedures

#### 4.1. General experimental protocol

All chemicals were purchased at the highest commercial quality and used without further purification, unless otherwise stated. Reactions were monitored by thin-layer chromatography (TLC) carried out on Sigma Aldrich silica gel plates (60 F254) using UV light as visualizing agent. Sigma Aldrich silica gel 63–200 mesh size was used for column chromatography. <sup>1</sup>H (400 MHz), <sup>13</sup>C (101 MHz) nuclear magnetic resonance spectra were recorded at ambient temperature on Bruker Avance III HD and <sup>1</sup>H (300 MHz) on Varian Mercury-VX. Chemical shifts ( $\delta$ ) are reported in parts per million (ppm) and coupling constants (*J*) are given in hertz (Hz). The following abbreviations were used to explain the multiplicities: s = singlet, d = doublet, dd = doublet of doublets, m = multiplet. UPLC-MS spectra were obtained by Shimadzu UFLC system equipped with Waters Acquity UPLC HSS C18 (50 mm  $\times$  2.1 mm  $\times$  1.8  $\mu$ m)

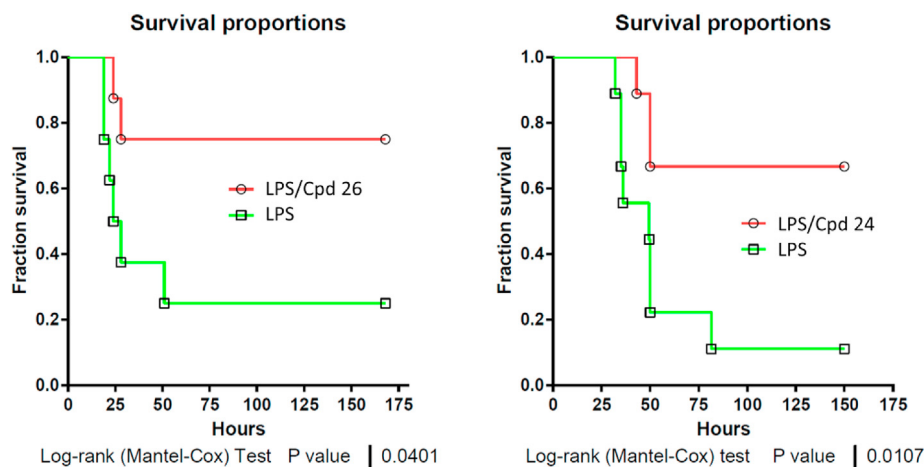


**Fig. 8.** Compound **24** and **26** improve mice survival in endotoxin-induced septic shock. Mice were treated *per os* with compound **26** (25 mg/kg) or **24** (75 mg/kg), and 2 h later LPS (20 mg/kg) was given *i.p.* to mice to assess effects of LPS on survival rate. Compounds **26** and **24** were given every 12 h following LPS injection during the experiment. The mice survival rate was evaluated using Kaplan–Meier curves (*n* = 8).

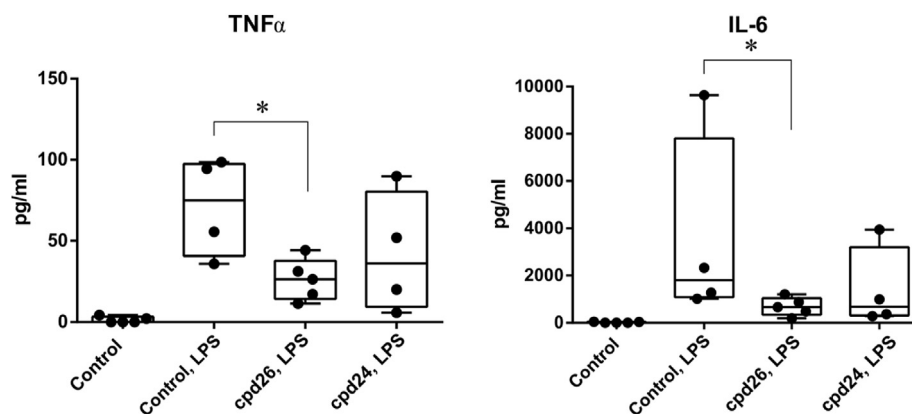


**Fig. 9.** Compound **26**, but not **24** reduces levels of TNF $\alpha$  and IL-6 in serum upon endotoxin challenge. Mice were treated *per os* with either compound **26** (50 mg/kg) or **24** (75 mg/kg), and 1 h later LPS (20 mg/kg) was given *i.p.* Additional drugs doses were administrated 12 h and 24 h following initial treatment and mice were scarified 4 h later with serum collection for downstream analyses. Cytokines levels were measured with Mouse Cytokine Magnetic Panel on Luminex platform. \* $p < 0.05$ ; Mann-Whitney  $U$  test.

column using flow rate of 0.5 mL/min. A gradient of water/acetonitrile with 0.1% of formic acid was used as an eluent. LC-MS analyses were performed on Bruker Amazon SL. Analytical separation was carried out on Waters Symmetry column C18  $3.9 \times 150$  mm  $5 \mu\text{m}$  using flow rate of 1.0 mL/min (ROTT-C18 – method A) or flow rate of 1.2 mL/min (BCM-30 – method C) with detection at 254 nm or on Kinetex XB C18  $4.6 \times 50$  mm  $2.6 \mu\text{m}$  column using flow rate of 0.5 mL/min (Kinetex-BCM – method B). The mobile phase was water (solvent A) and acetonitrile (solvent B) both containing 0.1% formic acid. Purity of the tested compounds ( $\geq 90\%$ ) was determined using these methods. HRMS analysis was performed on a Q Exactive™ Focus Hybrid Quadrupole-Orbitrap™ Mass Spectrometer. Yields refer to chromatographically and spectroscopically pure compounds unless otherwise stated.

## 4.2. Synthesis

The synthesis of the final compounds **1–28** and their intermediates **30, 35–37** will be described below. The synthesis of the remaining intermediates **29, 31a–d–34a–e** can be found in the Supporting Information.

### 4.2.1. General Procedure A for the synthesis of compounds **2–17, 20, 22–28** and **35–37**. Suzuki coupling

To a solution of corresponding boronic ester/acid (2.0 eq.) in a mixture of 1,4-dioxane/water (2/1) and caesium carbonate (2.5 eq.) in a microwave vial was added suitable halide (1.0 eq.) and [1,1'-bis(diphenylphosphino)ferrocene] palladium(II) chloride complex with dichloromethane (0.03 eq.). The reaction mixture was heated at 125 °C for 30 min under microwave irradiation. The reaction mixture was filtered through Celite, washed with EtOAc and concentrated in vacuo. The crude product was purified by flash chromatography (dichloromethane/methanol 95/5) to afford proper product.

### 4.2.2. General Procedure B for the synthesis of compounds **18** and **19**. Hydrolysis of nitrile

To a stirred solution of the corresponding nitrile (1.0 eq.) in a mixture of methanol/water (5/1) potassium carbonate (6.0 eq.) was added. After cooling to 0 °C 30% aqueous solution of hydrogen peroxide (23.0 eq.) was added dropwise and the reaction mixture was allowed to reach room temperature and stirred overnight. Methanol was evaporated and the reaction mixture was diluted with EtOAc. The layers were separated and the aqueous layer was further extracted with EtOAc. The organic layers were combined,

dried over  $\text{Na}_2\text{SO}_4$ , filtered off and concentrated. The crude product was purified by column chromatography on silica gel (dichloromethane/methanol 9/1) to give a proper amide.

**1-Benzyl-5-[5-bromo-1H-pyrazolo[3,4-b]pyridine-3-yl]pyridine-2(1H)-one (1)**. Trifluoroacetic acid (2 mL) was added to a solution of compound **30** (90 mg, 0.14 mmol) in dichloromethane (2 mL). The reaction mixture was stirred at room temperature overnight and then evaporated to dryness. The crude product was purified by flash chromatography (dichloromethane/methanol 95/5) to afford **1** (35 mg, 64%) as a light yellow solid:  $^1\text{H NMR}$  (400 MHz,  $\text{DMSO-}d_6$ )  $\delta$  13.96 (s, 1H), 8.86 (d,  $J = 2.1$  Hz, 1H), 8.63 (d,  $J = 2.1$  Hz, 1H), 8.51 (d,  $J = 2.6$  Hz, 1H), 8.12 (dd,  $J = 9.5, 2.6$  Hz, 1H), 7.36 (d,  $J = 4.3$  Hz, 4H), 7.32–7.25 (m, 1H), 6.60 (d,  $J = 9.5$  Hz, 1H), 5.30 (s, 2H);  $^{13}\text{C NMR}$  (101 MHz,  $\text{DMSO-}d_6$ )  $\delta$  161.2, 151.5, 149.9, 139.5, 138.9, 137.8, 137.3, 132.8, 129.0, 128.0, 127.9, 121.0, 113.1, 112.4, 112.1, 52.0; m.p.  $>270$  °C decomp.; LC-MS ( $m/z$ ) 381.3 ( $\text{M}+\text{H}^+$ ); HPLC purity (method B): 100%,  $t_R = 6.5$  min.

**1-Benzyl-5-(1H-indazol-6-yl)-1,2-dihydropyridin-2(1H)-one (2)**. Synthesized as described in the General Procedure A using 6-(4,4,5,5-tetramethyl-1,3,2-dioxaborolan-2-yl)-1H-indazole and 1-benzyl-5-bromo-1,2-dihydropyridin-2(1H)-one in 63% yield as a beige amorphous solid:  $^1\text{H NMR}$  (400 MHz,  $\text{DMSO-}d_6$ )  $\delta$  13.11 (s, 1H), 8.33 (d,  $J = 2.7$  Hz, 1H), 8.07 (s, 1H), 7.93 (dd,  $J = 9.4, 2.7$  Hz, 1H), 7.81 (d,  $J = 8.4$  Hz, 1H), 7.64 (s, 1H), 7.47–7.24 (m, 6H), 6.56 (d,  $J = 9.4$  Hz, 1H), 5.22 (s, 2H);  $^{13}\text{C NMR}$  (101 MHz,  $\text{DMSO-}d_6$ )  $\delta$  161.1, 140.9, 140.0, 137.9, 137.2, 134.4, 133.9, 129.0, 128.2, 128.0, 122.3, 121.5, 120.5, 119.3, 119.2, 106.7, 52.0; LC-MS ( $m/z$ ) 302.1 ( $\text{M}+\text{H}^+$ ); HPLC purity (method C): 100%,  $t_R = 7.8$  min.

**1-Benzyl-5-(1H-indol-6-yl)-1,2-dihydropyridin-2(1H)-one (3)**. Synthesized as described in the General Procedure A using boronic ester/acid **29** and 6-bromoindole in 26% yield as a yellow solid:  $^1\text{H NMR}$  (400 MHz,  $\text{DMSO-}d_6$ )  $\delta$  11.13 (s, 1H), 8.16 (d,  $J = 2.6$  Hz, 1H), 7.85 (dd,  $J = 9.4, 2.7$  Hz, 1H), 7.58 (d,  $J = 8.2$  Hz, 1H), 7.51 (s, 1H), 7.41–7.32 (m, 5H), 7.32–7.25 (m, 1H), 7.22–7.16 (m, 1H), 6.54 (d,  $J = 9.4$  Hz, 1H), 6.43 (s, 1H), 5.22 (s, 2H);  $^{13}\text{C NMR}$  (101 MHz,  $\text{DMSO-}d_6$ )  $\delta$  161.0, 140.2, 138.0, 136.9, 136.0, 129.5, 129.0, 128.2, 127.9, 127.3, 126.5, 120.9, 120.4, 117.6, 108.6, 101.4, 51.8; m.p. 110–112 °C; LC-MS ( $m/z$ ) 300.8 ( $\text{M}+\text{H}^+$ ); HPLC purity (method B): 99%,  $t_R = 7.0$  min.

**1-Benzyl-5-(1-methyl-1H-indazol-6-yl)-1,2-dihydropyridin-2(1H)-one (4)**. Synthesized as described in the General Procedure A using boronic ester/acid **29** and 6-bromo-1-methyl-1H-indazole in 43% yield as a brown oil:  $^1\text{H NMR}$  (400 MHz,  $\text{DMSO-}d_6$ )  $\delta$  8.37 (d,  $J = 2.7$  Hz, 1H), 8.02 (d,  $J = 10.7$  Hz, 2H), 7.85 (s, 1H), 7.79 (d,  $J = 8.4$  Hz, 1H), 7.40–7.33 (m, 5H), 7.33–7.24 (m, 1H), 6.59 (d,

$J = 9.5$  Hz, 1H), 5.22 (s, 2H), 4.08 (s, 3H);  $^{13}\text{C}$  NMR (101 MHz, DMSO- $d_6$ )  $\delta$  161.2, 140.7, 140.0, 137.8, 137.3, 134.3, 132.7, 129.0, 128.1, 128.0, 122.8, 121.7, 120.4, 119.1, 119.0, 106.3, 52.1, 35.8; LC-MS ( $m/z$ ) 316.3 (M+H) $^+$ ; HPLC purity (method C): 99%,  $t_R = 9.4$  min.

**1-Benzyl-5-(2-methyl-2H-indazol-6-yl)-1,2-dihydropyridin-2(1H)-one (5)**. Synthesized as described in the General Procedure A using boronic ester/acid **29** and 6-bromo-2-methyl-2H-indazole in 43% yield as a brown amorphous solid:  $^1\text{H}$  NMR (400 MHz, DMSO- $d_6$ )  $\delta$  8.37 (d,  $J = 2.7$  Hz, 1H), 8.05–7.98 (m, 2H), 7.84 (d,  $J = 1.3$  Hz, 1H), 7.81–7.76 (m, 1H), 7.42–7.31 (m, 5H), 7.34–7.24 (m, 1H), 6.59 (d,  $J = 9.5$  Hz, 1H), 5.22 (s, 2H), 4.08 (s, 3H);  $^{13}\text{C}$  NMR (101 MHz, DMSO- $d_6$ )  $\delta$  161.2, 140.7, 140.0, 137.8, 137.3, 134.3, 132.7, 129.0, 128.1, 128.0, 122.8, 121.7, 120.4, 119.1, 119.0, 106.3, 52.1, 35.8; LC-MS ( $m/z$ ) 316.3 (M+H) $^+$ ; HPLC purity (method B): 97%,  $t_R = 6.4$  min.

**5-(1H-Indazol-6-yl)-1-(2-phenylethyl)-1,2-dihydropyridin-2(1H)-one (6)**. Synthesized as described in the General Procedure A using boronic ester/acid **32a** and 6-bromo-1H-indazole in 42% yield as a beige amorphous solid:  $^1\text{H}$  NMR (400 MHz, DMSO- $d_6$ )  $\delta$  13.11 (s, 1H), 8.06 (s, 1H), 7.94 (d,  $J = 2.7$  Hz, 1H), 7.86 (dd,  $J = 9.3, 2.7$  Hz, 1H), 7.77 (d,  $J = 8.4$  Hz, 1H), 7.51 (s, 1H), 7.38–7.22 (m, 5H), 7.20 (dd,  $J = 8.5, 1.3$  Hz, 1H), 6.52 (d,  $J = 9.4$  Hz, 1H), 4.27–4.18 (m, 2H), 3.06–2.98 (m, 2H); LC-MS ( $m/z$ ) 316.3 (M+H) $^+$ ; HPLC purity (method C): 95%,  $t_R = 8.3$  min.

**5-(1H-Indazol-6-yl)-1-(2-oxo-2-phenylethyl)-1,2-dihydropyridin-2(1H)-one (7)**. Synthesized as described in the General Procedure A using boronic ester/acid **32b** and 6-bromo-1H-indazole in 32% yield as a light brown solid:  $^1\text{H}$  NMR (400 MHz, DMSO- $d_6$ )  $\delta$  13.13 (s, 1H), 8.21 (d,  $J = 2.7$  Hz, 1H), 8.13–8.06 (m, 3H), 8.00 (dd,  $J = 9.5, 2.7$  Hz, 1H), 7.82 (d,  $J = 8.5$  Hz, 1H), 7.77–7.72 (m, 1H), 7.68–7.59 (m, 3H), 7.33 (dd,  $J = 8.5, 1.5$  Hz, 1H), 6.58 (d,  $J = 9.5$  Hz, 1H), 5.61 (s, 2H);  $^{13}\text{C}$  NMR (101 MHz, DMSO- $d_6$ )  $\delta$  193.3, 161.1, 141.0, 140.3, 138.2, 135.1, 134.5, 133.9, 129.4, 128.4, 122.3, 121.6, 119.9, 119.2, 118.7, 106.5, 55.6; m.p. >210 °C decomp.; LC-MS ( $m/z$ ) 330.1 (M+H) $^+$ ; HPLC purity (method C): 94%,  $t_R = 7.2$  min.

**5-(1H-Indazol-6-yl)-1-(morpholine-4-carbonyl)-1,2-dihydropyridin-2(1H)-one (8)**. Synthesized as described in the General Procedure A using 6-(4,4,5,5-tetramethyl-1,3,2-dioxaborolan-2-yl)-1H-indazole and pyridinone **31c** in 53% yield as a brown amorphous solid:  $^1\text{H}$  NMR (400 MHz, DMSO- $d_6$ )  $\delta$  13.24 (s, 1H), 8.71 (d,  $J = 2.6$  Hz, 1H), 8.28 (dd,  $J = 8.4, 2.6$  Hz, 1H), 8.14 (s, 1H), 7.89 (d,  $J = 8.4$  Hz, 1H), 7.83 (s, 1H), 7.47 (dd,  $J = 8.4, 1.3$  Hz, 1H), 7.31 (d,  $J = 8.4$  Hz, 1H), 3.71–3.65 (m, 4H), 3.63 (s, 2H), 3.46 (s, 2H); LC-MS ( $m/z$ ) 325.1 (M+H) $^+$ ; HPLC purity (method C): 90%,  $t_R = 6.3$  min.

**5-(1H-Indazol-6-yl)-1-methyl-1,2-dihydropyridin-2(1H)-one (9)**. Synthesized as described in the General Procedure A using boronic ester/acid **32c** and 6-bromo-1H-indazole in 53% yield as a brown amorphous solid:  $^1\text{H}$  NMR (400 MHz, DMSO- $d_6$ )  $\delta$  13.11 (s, 1H), 8.19 (d,  $J = 2.7$  Hz, 1H), 8.07 (s, 1H), 7.89 (dd,  $J = 9.4, 2.7$  Hz, 1H), 7.80 (d,  $J = 8.4$  Hz, 1H), 7.65 (s, 1H), 7.34 (dd,  $J = 8.5, 1.6$  Hz, 1H), 6.51 (d,  $J = 9.4$  Hz, 1H), 3.54 (s, 3H);  $^{13}\text{C}$  NMR (101 MHz, DMSO- $d_6$ )  $\delta$  161.6, 141.0, 139.7, 138.2, 134.6, 133.9, 122.3, 121.5, 119.6, 119.3, 118.6, 106.5, 37.5; LC-MS ( $m/z$ ) 226.0 (M+H) $^+$ ; HPLC purity (method C): 96%,  $t_R = 3.3$  min.

**1-[(2-Fluorophenyl)methyl]-5-(1H-indazol-6-yl)-1,2-dihydropyridin-2(1H)-one (10)**. Synthesized as described in the General Procedure A using 6-(4,4,5,5-tetramethyl-1,3,2-dioxaborolan-2-yl)-1H-indazole and pyridinone **33a** in 30% yield as a beige solid:  $^1\text{H}$  NMR (400 MHz, DMSO- $d_6$ )  $\delta$  13.12 (s, 1H), 8.27 (d,  $J = 2.7$  Hz, 1H), 8.07 (t,  $J = 1.3$  Hz, 1H), 7.96 (dd,  $J = 9.5, 2.7$  Hz, 1H), 7.81 (d,  $J = 8.4$  Hz, 1H), 7.69–7.63 (m, 1H), 7.40–7.31 (m, 2H), 7.27–7.15 (m, 3H), 6.56 (d,  $J = 9.5$  Hz, 1H), 5.27 (s, 2H);  $^{13}\text{C}$  NMR (101 MHz, DMSO- $d_6$ )  $\delta$  161.1, 160.6 (d,  $J = 245.2$  Hz), 141.0, 140.3, 137.5, 134.4, 133.90, 130.1 (d,  $J = 4.4$  Hz), 130.0 (d,  $J = 3.1$  Hz), 125.0

(d,  $J = 3.4$  Hz), 124.4 (d,  $J = 14.6$  Hz), 122.4, 121.6, 120.4, 119.2, 119.1, 115.8 (d,  $J = 21.0$  Hz), 106.7, 46.8; m.p. 173–175 °C; LC-MS ( $m/z$ ) 320.0 (M+H) $^+$ ; HPLC purity (method C): 99%,  $t_R = 8.2$  min.

**1-[(3-Fluorophenyl)methyl]-5-(1H-indazol-6-yl)-1,2-dihydropyridin-2(1H)-one (11)**. Synthesized as described in the General Procedure A using 6-(4,4,5,5-tetramethyl-1,3,2-dioxaborolan-2-yl)-1H-indazole and pyridinone **33b** in 21% yield as a beige amorphous solid:  $^1\text{H}$  NMR (400 MHz, DMSO- $d_6$ )  $\delta$  13.14 (s, 1H), 8.37 (d,  $J = 2.7$  Hz, 1H), 8.07 (d,  $J = 1.2$  Hz, 1H), 7.95 (dd,  $J = 9.5, 2.7$  Hz, 1H), 7.81 (d,  $J = 8.4$  Hz, 1H), 7.66 (s, 1H), 7.41 (td,  $J = 8.1, 6.1$  Hz, 1H), 7.35 (dd,  $J = 8.5, 1.5$  Hz, 1H), 7.26–7.20 (m, 2H), 7.17–7.10 (m, 1H), 6.57 (d,  $J = 9.5$  Hz, 1H), 5.22 (s, 2H); LC-MS ( $m/z$ ) 320.0 (M+H) $^+$ ; HPLC purity (method C): 99%,  $t_R = 8.3$  min.

**1-[(2-Chlorophenyl)methyl]-5-(1H-indazol-6-yl)-1,2-dihydropyridin-2(1H)-one (12)**. Synthesized as described in the General Procedure A using 6-(4,4,5,5-tetramethyl-1,3,2-dioxaborolan-2-yl)-1H-indazole and pyridinone **33c** in 65% yield as a white amorphous solid:  $^1\text{H}$  NMR (400 MHz, DMSO- $d_6$ )  $\delta$  13.12 (s, 1H), 8.27 (d,  $J = 2.6$  Hz, 1H), 8.10–8.04 (m, 1H), 8.01 (dd,  $J = 9.5, 2.7$  Hz, 1H), 7.81 (d,  $J = 8.4$  Hz, 1H), 7.66 (s, 1H), 7.56–7.49 (m, 1H), 7.39–7.28 (m, 3H), 7.00–6.91 (m, 1H), 6.61 (d,  $J = 9.5$  Hz, 1H), 5.49 (s, 2H);  $^{13}\text{C}$  NMR (101 MHz, DMSO- $d_6$ )  $\delta$  161.1, 141.0, 140.4, 137.6, 134.8, 134.3, 133.9, 132.4, 129.9, 129.5, 128.4, 127.9, 122.4, 121.6, 120.5, 119.2, 106.7, 50.3; LC-MS ( $m/z$ ) 336.3 (M+H) $^+$ ; HPLC purity (method B): 99%,  $t_R = 6.3$  min.

**1-[(3-Chlorophenyl)methyl]-5-(1H-indazol-6-yl)-1,2-dihydropyridin-2(1H)-one (13)**. Synthesized as described in the General Procedure A using 6-(4,4,5,5-tetramethyl-1,3,2-dioxaborolan-2-yl)-1H-indazole and pyridinone **33d** in 7% yield as a brown amorphous solid:  $^1\text{H}$  NMR (400 MHz, DMSO- $d_6$ )  $\delta$  13.12 (s, 1H), 8.38 (d,  $J = 2.6$  Hz, 1H), 8.07 (s, 1H), 7.94 (dd,  $J = 9.5, 2.7$  Hz, 1H), 7.81 (d,  $J = 8.4$  Hz, 1H), 7.66 (s, 1H), 7.47 (s, 1H), 7.41–7.32 (m, 4H), 6.57 (d,  $J = 9.5$  Hz, 1H), 5.21 (s, 2H);  $^{13}\text{C}$  NMR (101 MHz, DMSO- $d_6$ )  $\delta$  161.1, 140.9, 140.3, 137.2, 134.3, 133.9, 133.5, 130.9, 128.2, 128.0, 127.0, 122.4, 121.5, 120.5, 119.4, 119.3, 106.7, 51.7, 40.0; LC-MS ( $m/z$ ) 336.2 (M+H) $^+$ ; HPLC purity (method C): 98%,  $t_R = 9.8$  min.

**1-[(3,4-Dichlorophenyl)methyl]-5-(1H-indazol-6-yl)-1,2-dihydropyridin-2(1H)-one (14)**. Synthesized as described in the General Procedure A using 6-(4,4,5,5-tetramethyl-1,3,2-dioxaborolan-2-yl)-1H-indazole and pyridinone **33e** in 60% yield as a brown amorphous solid:  $^1\text{H}$  NMR (400 MHz, DMSO- $d_6$ )  $\delta$  13.12 (s, 1H), 8.39 (d,  $J = 2.6$  Hz, 1H), 8.07 (s, 1H), 7.94 (dd,  $J = 9.5, 2.7$  Hz, 1H), 7.81 (d,  $J = 8.5$  Hz, 1H), 7.70 (d,  $J = 2.0$  Hz, 1H), 7.66 (s, 1H), 7.63 (d,  $J = 8.3$  Hz, 1H), 7.40 (dd,  $J = 8.3, 2.1$  Hz, 1H), 7.35 (dd,  $J = 8.4, 1.5$  Hz, 1H), 6.57 (d,  $J = 9.5$  Hz, 1H), 5.19 (s, 2H);  $^{13}\text{C}$  NMR (101 MHz, DMSO- $d_6$ )  $\delta$  161.1, 140.9, 140.4, 138.9, 137.2, 134.3, 133.9, 131.5, 131.2, 130.7, 130.6, 128.8, 122.4, 121.5, 120.5, 119.5, 119.3, 106.8, 51.3; LC-MS ( $m/z$ ) 371.4 (M+H) $^+$ ; HPLC purity (method C): 97%,  $t_R = 11.1$  min.

**5-(1H-Indazol-6-yl)-1-[[2-(trifluoromethyl)phenyl]methyl]-1,2-dihydropyridin-2(1H)-one (15)**. Synthesized as described in the General Procedure A using 6-(4,4,5,5-tetramethyl-1,3,2-dioxaborolan-2-yl)-1H-indazole and pyridinone **33f** in 48% yield as a beige solid:  $^1\text{H}$  NMR (400 MHz, DMSO- $d_6$ )  $\delta$  13.12 (s, 1H), 8.30 (d,  $J = 2.7$  Hz, 1H), 8.09–8.02 (m, 2H), 7.81 (d,  $J = 8.4$  Hz, 2H), 7.69 (s, 1H), 7.64 (t,  $J = 7.6$  Hz, 1H), 7.51 (t,  $J = 7.6$  Hz, 1H), 7.36 (dd,  $J = 8.5, 1.6$  Hz, 1H), 6.93 (d,  $J = 7.8$  Hz, 1H), 6.63 (d,  $J = 9.5$  Hz, 1H), 5.44 (s, 2H);  $^{13}\text{C}$  NMR (101 MHz, DMSO- $d_6$ )  $\delta$  161.1, 141.0, 140.6, 137.8, 136.1, 134.3, 133.9, 133.5, 128.1, 127.0, 126.6 (q,  $J = 5.2$  Hz), 126.2 (q,  $J = 30.4$  Hz), 124.9 (q,  $J = 273.9$  Hz), 122.4, 121.5, 120.6, 119.4, 119.3, 106.7, 49.3; m.p. >205 °C decomp.; LC-MS ( $m/z$ ) 370.0 (M+H) $^+$ ; HPLC purity (method C): 98%,  $t_R = 10.5$  min.

**5-(1H-Indazol-6-yl)-1-[[3-(trifluoromethyl)phenyl]methyl]-1,2-dihydropyridin-2(1H)-one (16)**. Synthesized as described in the General Procedure A using 6-(4,4,5,5-tetramethyl-1,3,2-

dioxaborolan-2-yl)-1*H*-indazole and pyridinone **33g** in 66% yield as a red amorphous solid:  $^1\text{H NMR}$  (400 MHz, DMSO- $d_6$ )  $\delta$  13.12 (s, 1H), 8.43 (d,  $J = 2.7$  Hz, 1H), 8.08 (s, 1H), 7.95 (dd,  $J = 9.5, 2.7$  Hz, 1H), 7.84–7.78 (m, 2H), 7.72–7.65 (m, 3H), 7.60 (t,  $J = 7.7$  Hz, 1H), 7.35 (dd,  $J = 8.5, 1.5$  Hz, 1H), 6.58 (d,  $J = 9.5$  Hz, 1H), 5.30 (s, 2H);  $^{13}\text{C NMR}$  (101 MHz, DMSO- $d_6$ )  $\delta$  161.2, 140.9, 140.3, 139.2, 137.3, 134.3, 133.9, 132.4, 130.1, 129.6 (q,  $J = 31.6$  Hz), 125.1 (q,  $J = 3.8$  Hz), 124.8 (q,  $J = 3.9$  Hz), 124.6 (q,  $J = 272.4$  Hz), 122.4, 121.5, 120.5, 119.4, 119.3, 106.8, 51.9; LC-MS ( $m/z$ ) 370.1 (M+H) $^+$ ; HPLC purity (method C): 98%,  $t_R = 10.6$  min.

5-(1*H*-Indazol-6-yl)-1-[[4-(trifluoromethyl)phenyl]methyl]-1,2-dihydropyridin-2(1*H*)-one (**17**). Synthesized as described in the General Procedure A using 6-(4,4,5,5-tetramethyl-1,3,2-dioxaborolan-2-yl)-1*H*-indazole and pyridinone **33h** in 40% yield as a beige amorphous solid:  $^1\text{H NMR}$  (400 MHz, DMSO- $d_6$ )  $\delta$  13.12 (s, 1H), 8.39 (d,  $J = 2.6$  Hz, 1H), 8.07 (s, 1H), 7.96 (dd,  $J = 9.5, 2.6$  Hz, 1H), 7.81 (d,  $J = 8.4$  Hz, 1H), 7.73 (d,  $J = 8.1$  Hz, 2H), 7.67 (s, 1H), 7.58 (d,  $J = 8.0$  Hz, 2H), 7.35 (dd,  $J = 8.5, 1.4$  Hz, 1H), 6.58 (d,  $J = 9.5$  Hz, 1H), 5.31 (s, 2H);  $^{13}\text{C NMR}$  (101 MHz, DMSO- $d_6$ )  $\delta$  161.1, 142.5, 140.9, 140.3, 137.4, 134.3, 133.9, 128.9, 125.9 (q,  $J = 4.1$  Hz), 122.4, 121.5, 120.5, 119.4, 119.3, 106.7, 51.9; LC-MS ( $m/z$ ) 370.1 (M+H) $^+$ ; HPLC purity (method C): 94%,  $t_R = 10.8$  min.

2-[[5-(1*H*-Indazol-6-yl)-2-oxo-1,2-dihydropyridin-1-yl]methyl]benzamide (**18**). Synthesized as described in the General Procedure B using nitrile **35** in 46% yield as a brown amorphous solid:  $^1\text{H NMR}$  (400 MHz, DMSO- $d_6$ )  $\delta$  13.10 (s, 1H), 8.33 (d,  $J = 2.7$  Hz, 1H), 8.09 (s, 1H), 8.09–8.04 (m, 1H), 7.96 (dd,  $J = 9.4, 2.7$  Hz, 1H), 7.80 (dd,  $J = 8.5, 0.8$  Hz, 1H), 7.65 (s, 1H), 7.59–7.54 (m, 2H), 7.41 (td,  $J = 7.5, 1.6$  Hz, 1H), 7.40–7.29 (m, 2H), 7.11 (dd,  $J = 7.6, 1.3$  Hz, 1H), 6.57 (d,  $J = 9.4$  Hz, 1H), 5.41 (s, 2H);  $^{13}\text{C NMR}$  (101 MHz, DMSO- $d_6$ )  $\delta$  170.9, 161.4, 140.1, 137.8, 136.0, 135.9, 134.4, 130.6, 128.2, 128.1, 127.6, 122.3, 121.5, 120.4, 119.2, 119.1, 106.7, 50.1; LC-MS ( $m/z$ ) 345.2 (M+H) $^+$ ; HPLC purity (method C): 96%,  $t_R = 4.8$  min.

4-[[5-(1*H*-Indazol-6-yl)-2-oxo-1,2-dihydropyridin-1-yl]methyl]benzamide (**19**). Synthesized as described in the General Procedure B using nitrile **36** in 72% yield as a white amorphous solid:  $^1\text{H NMR}$  (400 MHz, DMSO- $d_6$ )  $\delta$  13.17 (s, 1H), 8.34 (d,  $J = 2.7$  Hz, 1H), 8.07 (s, 1H), 7.97–7.91 (m, 2H), 7.88–7.77 (m, 3H), 7.66 (s, 1H), 7.43 (d,  $J = 8.0$  Hz, 2H), 7.37–7.31 (m, 2H), 6.57 (d,  $J = 9.4$  Hz, 1H), 5.26 (s, 2H);  $^{13}\text{C NMR}$  (101 MHz, DMSO- $d_6$ )  $\delta$  168.0, 161.1, 141.0, 140.9, 140.2, 137.3, 134.3, 134.0, 133.8, 128.2, 127.9, 122.3, 121.5, 120.5, 119.3, 106.8, 51.9; LC-MS ( $m/z$ ) 345.0 (M+H) $^+$ ; HPLC purity (method A): 99%,  $t_R = 13.4$  min.

3-[[5-(1*H*-Indazol-6-yl)-2-oxo-1,2-dihydropyridin-1-yl]methyl]benzamide (**20**). Synthesized as described in the General Procedure A using 6-(4,4,5,5-tetramethyl-1,3,2-dioxaborolan-2-yl)-1*H*-indazole and pyridinone **33k** in 70% yield as a brown solid:  $^1\text{H NMR}$  (400 MHz, DMSO- $d_6$ )  $\delta$  13.11 (s, 1H), 8.35 (d,  $J = 2.7$  Hz, 1H), 8.07 (s, 1H), 7.97 (s, 1H), 7.94 (dd,  $J = 9.5, 2.7$  Hz, 1H), 7.89 (s, 1H), 7.80 (t,  $J = 8.4$  Hz, 2H), 7.66 (s, 1H), 7.52 (dt,  $J = 7.8, 1.4$  Hz, 1H), 7.43 (t,  $J = 7.6$  Hz, 1H), 7.38–7.32 (m, 2H), 6.57 (d,  $J = 9.5$  Hz, 1H), 5.26 (s, 2H);  $^{13}\text{C NMR}$  (101 MHz, DMSO- $d_6$ )  $\delta$  168.1, 161.1, 141.0, 140.1, 138.0, 137.3, 135.1, 134.4, 133.9, 131.0, 128.9, 127.6, 126.9, 122.3, 121.5, 120.5, 119.3, 119.2, 106.7, 52.0; m.p. > 220 °C decomp.; LC-MS ( $m/z$ ) 345.1 (M+H) $^+$ ; HPLC purity (method C): 95%,  $t_R = 4.4$  min.

1-[(3-Aminophenyl)methyl]-5-(1*H*-indazol-6-yl)-1,2-dihydropyridin-2(1*H*)-one (**21**). To a Boc-protected compound **37** (86 mg, 0.20 mmol) 4 M HCl in 1,4-dioxane was added (2 mL). After stirring at room temperature for 3 h, the reaction mixture was diluted with water, neutralized with saturated aqueous solution of NaHCO<sub>3</sub> and extracted with EtOAc (three times). The organic layers were combined, dried over MgSO<sub>4</sub>, filtered off and concentrated. The crude product was purified by column chromatography on silica gel (dichloromethane/methanol 9/1) to give **21** as a white amorphous solid (41 mg, 89%):  $^1\text{H NMR}$  (400 MHz, DMSO- $d_6$ )

$\delta$  13.10 (s, 1H), 8.19 (d,  $J = 2.7$  Hz, 1H), 8.07 (s, 1H), 7.91 (dd,  $J = 9.4, 2.7$  Hz, 1H), 7.80 (d,  $J = 8.4$  Hz, 1H), 7.63 (s, 1H), 7.32 (dd,  $J = 8.5, 1.5$  Hz, 1H), 6.98 (t,  $J = 7.7$  Hz, 1H), 6.59–6.43 (m, 4H), 5.09 (s, 2H), 5.07 (s, 2H);  $^{13}\text{C NMR}$  (101 MHz, DMSO- $d_6$ )  $\delta$  161.1, 149.4, 141.0, 139.8, 138.5, 137.2, 134.5, 133.9, 129.5, 122.3, 121.5, 120.4, 119.3, 118.9, 115.4, 113.6, 113.2, 106.6, 51.9; LC-MS ( $m/z$ ) 317.2 (M+H) $^+$ ; HPLC purity (method C): 99%,  $t_R = 11.8$  min.

*N*-[3-[[5-(1*H*-Indazol-6-yl)-2-oxo-1,2-dihydropyridin-1-yl]methyl]phenyl]acetamide (**22**). Synthesized as described in the General Procedure A using 6-(4,4,5,5-tetramethyl-1,3,2-dioxaborolan-2-yl)-1*H*-indazole and pyridinone **33n** in 62% yield as a light yellow solid:  $^1\text{H NMR}$  (400 MHz, DMSO- $d_6$ )  $\delta$  13.13 (s, 1H), 9.96 (s, 1H), 8.30 (d,  $J = 2.7$  Hz, 1H), 8.07 (s, 1H), 7.94 (dd,  $J = 9.5, 2.7$  Hz, 1H), 7.81 (d,  $J = 8.4$  Hz, 1H), 7.65 (s, 1H), 7.60–7.54 (m, 1H), 7.48 (t,  $J = 1.8$  Hz, 1H), 7.34 (dd,  $J = 8.4, 1.5$  Hz, 1H), 7.27 (t,  $J = 7.9$  Hz, 1H), 7.04 (d,  $J = 7.6$  Hz, 1H), 6.56 (d,  $J = 9.5$  Hz, 1H), 5.19 (s, 2H), 2.01 (s, 3H); m.p. 132–135 °C; LC-MS ( $m/z$ ) 359.3 (M+H) $^+$ ; HPLC purity (method A): 99%,  $t_R = 14.6$  min.

5-(3-Amino-1*H*-indazol-6-yl)-1-benzyl-1,2-dihydropyridin-2(1*H*)-one (**23**). Synthesized as described in the General Procedure A using boronic ester/acid **29** and 3-amino-6-bromo-1*H*-indazole in 43% yield as a white solid:  $^1\text{H NMR}$  (400 MHz, DMSO- $d_6$ )  $\delta$  11.43 (s, 1H), 8.27 (d,  $J = 2.7$  Hz, 1H), 7.88 (dd,  $J = 9.5, 2.7$  Hz, 1H), 7.72 (d,  $J = 8.4$  Hz, 1H), 7.40–7.32 (m, 4H), 7.35–7.24 (m, 2H), 7.11 (dd,  $J = 8.3, 1.5$  Hz, 1H), 6.54 (d,  $J = 9.4$  Hz, 1H), 5.36 (s, 2H), 5.21 (s, 2H);  $^{13}\text{C NMR}$  (101 MHz, DMSO- $d_6$ )  $\delta$  161.2, 158.9, 158.5, 147.6, 143.0, 139.8, 137.8, 137.6, 137.3, 129.0, 128.2, 128.0, 122.1, 120.5, 118.7, 118.2, 112.4, 106.7, 52.0; m.p. 210–213 °C; LC-MS ( $m/z$ ) 317.2 (M+H) $^+$ ; HPLC purity (method C): 100%,  $t_R = 4.2$  min.

5-(3-Amino-1*H*-indazol-6-yl)-1-[(2-fluorophenyl)methyl]-1,2-dihydropyridin-2(1*H*)-one (**24**). Synthesized as described in the General Procedure A using boronic ester/acid **34a** and 3-amino-6-bromo-1*H*-indazole in 57% yield as a beige solid:  $^1\text{H NMR}$  (400 MHz, DMSO- $d_6$ )  $\delta$  11.45 (s, 1H), 8.22 (d,  $J = 2.7$  Hz, 1H), 7.92 (dd,  $J = 9.5, 2.7$  Hz, 1H), 7.73 (d,  $J = 8.4$  Hz, 1H), 7.39–7.32 (m, 2H), 7.27–7.20 (m, 1H), 7.20–7.16 (m, 2H), 7.11 (dd,  $J = 8.4, 1.5$  Hz, 1H), 6.54 (d,  $J = 9.5$  Hz, 1H), 5.37 (s, 2H), 5.26 (s, 2H);  $^{13}\text{C NMR}$  (101 MHz, DMSO- $d_6$ )  $\delta$  161.1, 160.6 (d,  $J = 245.1$  Hz), 149.6, 142.5, 140.3, 137.3, 134.4, 130.0 (d,  $J = 8.4$  Hz), 130.0 (d,  $J = 4.0$  Hz), 125.0 (d,  $J = 3.3$  Hz), 124.4 (d,  $J = 14.6$  Hz), 121.4, 120.3, 119.4, 116.3, 115.8 (d,  $J = 21.0$  Hz), 113.6, 106.1, 46.8; m.p. 209–212 °C; LC-MS ( $m/z$ ) 335.3 (M+H) $^+$ ; HPLC purity (method C): 99%,  $t_R = 4.7$  min.

5-(3-Amino-1*H*-indazol-6-yl)-1-[(3-fluorophenyl)methyl]-1,2-dihydropyridin-2(1*H*)-one (**25**). Synthesized as described in the General Procedure A using boronic ester/acid **34b** and 3-amino-6-bromo-1*H*-indazole in 72% yield as a brown solid:  $^1\text{H NMR}$  (400 MHz, DMSO- $d_6$ )  $\delta$  11.45 (s, 1H), 8.31 (d,  $J = 2.6$  Hz, 1H), 7.90 (dd,  $J = 9.5, 2.7$  Hz, 1H), 7.73 (d,  $J = 8.4$  Hz, 1H), 7.40 (td,  $J = 8.2, 6.3$  Hz, 1H), 7.35 (dd,  $J = 1.5, 0.8$  Hz, 1H), 7.26–7.18 (m, 2H), 7.17–7.09 (m, 2H), 6.55 (d,  $J = 9.4$  Hz, 1H), 5.37 (s, 2H), 5.21 (s, 2H);  $^{13}\text{C NMR}$  (101 MHz, DMSO- $d_6$ )  $\delta$  162.6 (d,  $J = 243.7$  Hz), 161.1, 149.6, 142.5, 140.7 (d,  $J = 7.4$  Hz), 140.2, 137.0, 134.4, 131.0 (d,  $J = 8.3$  Hz), 124.3 (d,  $J = 2.7$  Hz), 121.3, 120.4, 119.7, 116.3, 115.1 (d,  $J = 21.9$  Hz), 114.8 (d,  $J = 20.9$  Hz), 113.6, 106.1, 51.6; m.p. 82–85 °C; LC-MS ( $m/z$ ) 335.2 (M+H) $^+$ ; HPLC purity (method C): 99%,  $t_R = 4.6$  min.

5-(3-amino-1*H*-indazol-6-yl)-1-[(3-chlorophenyl)methyl]-1,2-dihydropyridin-2(1*H*)-one (**26**). Synthesized as described in the General Procedure A using boronic ester/acid **34c** and 3-amino-6-bromo-1*H*-indazole in 78% yield as a grey solid:  $^1\text{H NMR}$  (400 MHz, DMSO- $d_6$ )  $\delta$  11.45 (s, 1H), 8.32 (d,  $J = 2.5$  Hz, 1H), 7.90 (dd,  $J = 9.5, 2.7$  Hz, 1H), 7.73 (d,  $J = 8.4$  Hz, 1H), 7.47 (br s, 1H), 7.42–7.33 (m, 4H), 7.13 (dd,  $J = 8.4, 1.5$  Hz, 1H), 6.55 (d,  $J = 9.5$  Hz, 1H), 5.36 (s, 2H), 5.20 (s, 2H);  $^{13}\text{C NMR}$  (101 MHz, DMSO- $d_6$ )  $\delta$  161.1, 149.6, 142.5, 140.3, 140.3, 137.0, 134.4, 133.5, 130.9, 128.2, 128.0, 127.0, 121.3, 120.4, 119.7, 116.3, 113.6, 106.1, 51.6; m.p. 175–177 °C; LC-MS ( $m/z$ )

350.9 (M+H)<sup>+</sup>; HPLC purity (method C): 100%, t<sub>R</sub> = 7.1 min; HRMS *m/z* [M+1]<sup>+</sup> calcd for C<sub>19</sub>H<sub>15</sub>ClN<sub>4</sub>O 351.1007, found 351.1007.

5-(3-Amino-1H-indazol-6-yl)-1-[[3-(trifluoromethyl)phenyl]methyl]-1,2-dihydropyridin-2(1H)-one (**27**). Synthesized as described in the General Procedure A using boronic ester/acid **34d** and 3-amino-6-bromo-1H-indazole in 22% yield as a brown amorphous solid: <sup>1</sup>H NMR (400 MHz, DMSO-*d*<sub>6</sub>) δ 11.4 (s, 1H), 8.53 (d, *J* = 2.7 Hz, 1H), 8.03 (d, *J* = 8.6 Hz, 1H), 7.97 (dd, *J* = 9.5, 2.7 Hz, 1H), 7.79 (s, 1H), 7.68 (t, *J* = 6.9 Hz, 2H), 7.61 (d, *J* = 7.7 Hz, 1H), 7.58 (s, 1H), 7.43 (dd, *J* = 8.6, 1.5 Hz, 1H), 6.58 (d, *J* = 9.5 Hz, 1H), 5.43 (s, 2H), 5.30 (s, 2H); LC-MS (*m/z*) 385.1 (M+H)<sup>+</sup>; HPLC purity (method C): 91%, t<sub>R</sub> = 7.0 min.

*N*-(3-[[5-(3-Amino-1H-indazol-6-yl)-2-oxo-1,2-dihydropyridin-1-yl]methyl]phenyl)acetamide (**28**). Synthesized as described in the General Procedure A using boronic ester/acid **34e** and 3-amino-6-bromo-1H-indazole in 67% yield as a grey solid: <sup>1</sup>H NMR (400 MHz, DMSO-*d*<sub>6</sub>) δ 11.44 (s, 1H), 9.95 (s, 1H), 8.23 (d, *J* = 2.7 Hz, 1H), 7.89 (dd, *J* = 9.5, 2.7 Hz, 1H), 7.72 (d, *J* = 8.4 Hz, 1H), 7.57 (d, *J* = 7.9 Hz, 1H), 7.47 (d, *J* = 2.0 Hz, 1H), 7.34 (s, 1H), 7.26 (t, *J* = 7.9 Hz, 1H), 7.12 (dd, *J* = 8.4, 1.5 Hz, 1H), 7.03 (d, *J* = 7.6 Hz, 1H), 6.54 (d, *J* = 9.4 Hz, 1H), 5.36 (s, 2H), 5.18 (s, 2H), 2.01 (s, 3H); <sup>13</sup>C NMR (101 MHz, DMSO-*d*<sub>6</sub>) δ 168.8, 161.1, 149.6, 142.5, 140.0, 138.4, 137.0, 134.5, 129.3, 122.7, 121.3, 120.4, 119.4, 118.6, 118.4, 116.3, 113.6, 106.1, 51.9, 24.4; m.p. 148–153 °C; LC-MS (*m/z*) 374.1 (M+H)<sup>+</sup>; HPLC purity (method A): 100%, t<sub>R</sub> = 11.9 min.

1-Benzyl-5-[5-bromo-1-(triphenylmethyl)pyrazolo[3,4-*b*]pyridin-3-yl]pyridine-2(1H)-one (**30**). The boronic ester/acid **29** (100 mg, 0.44 mmol, 1.0 eq.) was dissolved in mixture of acetonitrile/toluene (2/1). Saturated aqueous solution of NaHCO<sub>3</sub> (1.5 mL), 5-bromo-3-iodo-1-(triphenylmethyl)pyrazolo[3,4-*b*]pyridine (170 mg, 0.31 mmol, 1.4 eq.) and [1,1'-bis(diphenylphosphino)ferrocene] palladium(II) chloride complex with dichloromethane (7 mg, 0.03 eq.) were added and reaction mixture was flushed with argon for 10 min. Then, the reaction mixture was heated at 60 °C for 7 h, after cooling to room temperature, filtered through Celite, washed with EtOAc and concentrated in vacuo. The crude product was purified by flash column chromatography (dichloromethane/methanol 99/1) to afford **30** (96 mg, 50%) as a beige amorphous solid: <sup>1</sup>H NMR (400 MHz, DMSO-*d*<sub>6</sub>) δ 8.86 (d, *J* = 2.1 Hz, 1H), 8.49 (d, *J* = 2.6 Hz, 1H), 8.37 (d, *J* = 2.2 Hz, 1H), 7.84 (dd, *J* = 9.5, 2.6 Hz, 1H), 7.35 (d, *J* = 3.7 Hz, 4H), 7.31–7.21 (m, 16H), 6.58 (d, *J* = 9.5 Hz, 1H), 5.28 (s, 2H); <sup>13</sup>C NMR (101 MHz, DMSO-*d*<sub>6</sub>) δ 161.2, 151.0, 148.8, 142.7, 138.7, 138.3, 137.8, 137.6, 133.0, 129.9, 129.0, 128.0, 127.9, 127.9, 127.4, 121.2, 115.7, 113.4, 111.6, 78.5, 52.0; UPLC (*m/z*) 625.0 (M+H)<sup>+</sup>; 97%, t<sub>R</sub> = 4.9 min.

2-[[5-(1H-Indazol-6-yl)-2-oxo-1,2-dihydropyridin-1-yl]methyl]benzotrile (**35**). Synthesized as described in the General Procedure A using 6-(4,4,5,5-tetramethyl-1,3,2-dioxaborolan-2-yl)-1H-indazole and pyridinone **33i** in 62% yield as a beige amorphous solid: <sup>1</sup>H NMR (400 MHz, DMSO-*d*<sub>6</sub>) δ 13.14 (s, 1H), 8.38 (d, *J* = 2.5 Hz, 1H), 8.08 (s, 1H), 8.01 (dd, *J* = 9.5, 2.7 Hz, 1H), 7.90 (d, *J* = 7.6 Hz, 1H), 7.82 (d, *J* = 8.4 Hz, 1H), 7.75–7.65 (m, 2H), 7.50 (t, *J* = 8.0 Hz, 1H), 7.37 (dd, *J* = 8.5, 1.3 Hz, 1H), 7.22 (d, *J* = 7.6 Hz, 1H), 6.58 (d, *J* = 9.5 Hz, 1H), 5.40 (s, 2H); LC-MS (*m/z*) 326.7 (M+H)<sup>+</sup>; HPLC purity (method B): 99%, t<sub>R</sub> = 5.5 min.

4-[[5-(1H-Indazol-6-yl)-2-oxo-1,2-dihydropyridin-1-yl]methyl]benzotrile (**36**). Synthesized as described in the General Procedure A using 6-(4,4,5,5-tetramethyl-1,3,2-dioxaborolan-2-yl)-1H-indazole and pyridinone **33j** in 61% yield as a beige amorphous solid: <sup>1</sup>H NMR (400 MHz, DMSO-*d*<sub>6</sub>) δ 13.12 (s, 1H), 8.38 (d, *J* = 2.6 Hz, 1H), 8.07 (s, 1H), 7.96 (dd, *J* = 9.5, 2.6 Hz, 1H), 7.89–7.78 (m, 3H), 7.67 (s, 1H), 7.54 (d, *J* = 8.1 Hz, 2H), 7.35 (d, *J* = 9.4 Hz, 1H), 6.58 (d, *J* = 9.5 Hz, 1H), 5.29 (s, 2H); <sup>13</sup>C NMR (101 MHz, DMSO-*d*<sub>6</sub>) δ 161.1, 143.4, 140.9, 140.4, 137.4, 134.3, 133.9, 132.9, 129.0, 122.4, 121.5, 120.5, 119.4, 119.3, 119.1, 110.7, 106.8, 52.1; LC-MS (*m/z*) 326.7

(M+H)<sup>+</sup>; HPLC purity (method B): 98%, t<sub>R</sub> = 5.5 min.

*tert*-Butyl *N*-(3-[[5-(1H-indazol-6-yl)-2-oxo-1,2-dihydropyridin-1-yl]methyl]phenyl)carbamate (**37**). Synthesized as described in the General Procedure A using 6-(4,4,5,5-tetramethyl-1,3,2-dioxaborolan-2-yl)-1H-indazole and pyridinone **33i** in 23% yield as a white amorphous solid: <sup>1</sup>H NMR (400 MHz, DMSO-*d*<sub>6</sub>) δ 13.11 (s, 1H), 9.34 (s, 1H), 8.26 (d, *J* = 2.7 Hz, 1H), 8.07 (s, 1H), 7.93 (dd, *J* = 9.5, 2.7 Hz, 1H), 7.80 (d, *J* = 8.4 Hz, 1H), 7.65 (s, 1H), 7.46 (s, 1H), 7.40–7.32 (m, 2H), 7.22 (t, *J* = 7.9 Hz, 1H), 6.94 (dt, *J* = 7.6, 1.3 Hz, 1H), 6.56 (d, *J* = 9.4 Hz, 1H), 5.17 (s, 2H), 1.45 (s, 9H); <sup>13</sup>C NMR (101 MHz, DMSO-*d*<sub>6</sub>) δ 161.1, 153.2, 141.0, 140.2, 140.0, 138.4, 137.3, 134.5, 133.9, 129.2, 122.3, 121.7, 121.5, 120.4, 119.3, 119.1, 117.8, 106.7, 79.5, 51.9, 28.6; LC-MS (*m/z*) 416.9 (M+H)<sup>+</sup>; HPLC purity (method B): 100%, t<sub>R</sub> = 6.7 min.

### 4.3. Biological section

#### 4.3.1. *In vitro* kinase assay

IC<sub>50</sub> experiments for MNK1 [Carna Bioscience, #02–145] were performed on white, 96-wells plate with 20 μM ATP [Promega] and 250 μM substrate peptide GRSRSRSR [Lipopharm]. Kinase reaction was run for 2 h at room temperature in assay buffer: 60 mM HEPES, 3 mM MgCl<sub>2</sub>, 3 mM MnCl<sub>2</sub>, 50 μg/ml PEG20, 3 μM sodium ortovanadate, 1 mM DTT, pH 7.5. ADP-Glo Kinase Assay kit [Promega, #V9103] was used to detect ADP produced in the kinase reaction. For inhibition constant (K<sub>i</sub>) experiments the compounds were tested in MNK1 reaction with 5 different ATP concentrations: 2 μM, 6 μM, 20 μM, 60 μM, 140 μM. IC<sub>50</sub> experiments for MNK2 [Carna Bioscience, #02–146] were performed on white, 96-wells plate with 100 μM ATP [Promega] and 160 μM substrate peptide GRSRSRSR [Lipopharm]. Kinase reaction was run for 2 h at room temperature in assay buffer was 50 mM MOPS, 5 mM MgCl<sub>2</sub>, 0.4 mM EDTA, 1 mM DTT, pH 7.5. ADP-Glo Kinase Assay kit [Promega, #V9103] was used to detect ADP produced in the kinase reaction. For inhibition constant experiments the compounds were tested in MNK2 reaction with 5 different ATP concentrations: 10 μM, 30 μM, 100 μM, 300 μM, 700 μM. IC<sub>50</sub> and inhibition constant values were determined by fitting variable slope (four parameters) model or competitive inhibition model, respectively, in GraphPad Prism 7.04 Software.

#### 4.3.2. Cell culture

MOLM-16 [DSMZ; ACC 555] cell line was cultured in RPMI 1640 containing 20% FBS, 1% pyruvate and 1% penicillin/streptomycin at 37 °C in a humidified incubator with 5% CO<sub>2</sub>. All media and Feta Bovine Serum (FBS) were purchased from Gibco.

#### 4.3.3. Western blot analysis

Compounds **24** and **26** were synthesized internally according to procedures described above. Drugs were dissolved in DMSO, and 10 mM aliquots were stored at -80 °C. The following commercially available antibodies were purchased from Cell Signaling Technology: phospho-eIF4e [Ser209, catalog 9741L], eIF4e [catalog 9742L]. b-Actin [catalog A2066] antibody was purchased from Sigma. Cells were treated with either compound **24** or **26** at the indicated times, and pellets were harvested to obtain protein extracts. Cell pellets were washed with cold PBS and lysed in ice-cold RIPA buffer with phosphatase inhibitors [Thermo Scientific, 89900]. After sonication, cell lysates were centrifuged at 16 900 g for 10 min. The supernatants were collected, and protein concentrations were determined using Bradford reagent [Sigma, B6916]. Equal amounts of protein in each well was resolved on MiniProtein Gels [Biorad, 456–8036] and transferred using Trans-Blot Turbo PVDF Transfer Packs [Biorad, 1704157]. Membranes were blocked for 40 min at room temperature in 5% fat-free milk, incubated with primary antibodies

overnight, washed 4 times in PBST, then incubated with HRP-conjugated secondary antibodies for 1 h at room temperature. After four PBST washes, blots were developed using ECL reagent [Biorad, 170–5061] on ChemiDoc (Biorad MP Imaging System). Quantitative image analysis was performed using ImageLab software (Biorad).

#### 4.3.4. Cytokine signaling pathways analysis

The level of cytokines in mouse serum samples were measured in duplicates using Cytokine & Chemokine 26-Plex Mouse ProcartaPlex™ Panel [Thermo Fisher; EPX260-26088-901.] on Luminex platform according to the manufacturer's recommendations.

#### 4.4. In vitro ADMET assays

##### 4.4.1. Metabolic stability assay

Metabolic stability assay was performed using mice microsomal fraction (phase I of metabolism) obtained from XenoTech. Compounds for metabolic stability testing were prepared as 10 mM stock solutions in DMSO. Compounds were incubated in triplicates at 1  $\mu$ M initial concentration with microsomal fraction in presence of NRS (NADPH-regenerating system, 1.3 mM). Final microsomal incubation (0.3 mg/ml) contained following components in phosphate buffer pH 7.4. Control incubations were conducted without cofactors. Reference compound – Verapamil was used as a positive control. Incubations were carried out for 1 h on 96 well plates using heated (+37 °C) orbital shaker (350 rpm). After the incubation, reaction was quenched by addition of cold acetonitrile. Plate containing samples was centrifuged at 2000 rpm for 15 min at 4 °C. Supernatants were analyzed using LC-MS technique. HPLC-MS consisted of a HPLC of the Dionex, Ultimate 3000 and mass spectrometer of Bruker Daltonics, amaZon SL (ESI-IT). Samples were analyzed in Single Ion Monitoring scan mode.

Percent loss of compound was calculated by normalization of peak area against time 0, where peak area at  $T_0$  is 100%. Elimination rate constant (h) was determined from the plot of ln (percent loss of compound) as a time function and equal minor value of linear curve slope. Half-life time was calculated from the following equation:

$$T_{1/2} = \frac{0.693}{k}$$

Calculated half-life time was used for intrinsic clearance calculation:

$$CL_{int} = \frac{V_d * 0.693}{T_{1/2}}$$

where,  $V_d$  – volume of distribution equals:

$$V_d = \frac{1}{\text{protein concentration} \left( \frac{\text{mg}}{\text{ml}} \right)}$$

##### 4.4.2. Kinetic solubility assay

The kinetic solubility assay is performed to determine the solubility of compounds in the *in vitro* assays conditions. Assay investigates solubility based on precipitation process. Compounds for kinetic solubility testing were prepared as 10 mM stock solutions in DMSO. Investigated compounds were diluted (in triplicates) with buffer of interest (water or Sørensen's buffer pH 7.4) to final concentration 500  $\mu$ M. Mixture was shaken on filter plate at 500 rpm for 1.5 h at RT. After incubation time filter plate was placed inside vacuum manifold and filtrated. Samples were collected and

concentration of filtrate was determined spectrophotometrically by measurement of UV-VIS absorption spectrum. Concentrations were calculated based on equations resulted from the calibration curves (in duplicates, 8 calibration points, dilution factor x2, 500  $\mu$ M  $\rightarrow$  3.91  $\mu$ M, including blank sample).

##### 4.4.3. Protein plasma binding assay

The assay of plasma protein binding was performed using Rapid Equilibrium Dialysis (RED) system of Thermo Scientific. Compounds for PPB testing were prepared as 10 mM stock solutions in DMSO. Plasma (human, mouse and rat) was spiked with investigated compound (in triplicates) at chosen initial concentration (5  $\mu$ M for compound **24**, 1  $\mu$ M for compound **26**) and transferred into plasma compartment of RED device. Dialysis was carried out against PBS buffer, pH 7.4, for 4 h at 37 °C, while agitating (300 rpm). Two reference compounds were used as control compounds: Warfarin and Metoprolol. After the incubation, samples were collected from both compartments. Plasma samples were spiked with aliquot volume of buffer, while buffer samples were spiked with aliquot volume of plasma to ensure a homogeneous matrix. 8-point calibration curves (dilution factor x2, including blank sample) were prepared in plasma spiked with buffer. Proteins were precipitated with the addition of cold acetonitrile, next samples were centrifuged at 2000 rpm for 15 min at 4 °C. Compound concentration was determined in both compartments using LC-MS technique. HPLC-MS consisted of a HPLC of the Dionex, Ultimate 3000 and mass spectrometer of Bruker Daltonics, amaZon SL (ESI-IT). Samples were analyzed in Single Ion Monitoring scan mode.

Based on concentration results from both compartments PPB was calculated.

$$\% \text{PPB} = \left( 1 - \frac{C_{\text{buffer}}}{C_{\text{plasma}}} \right) \times 100\%$$

##### 4.4.4. CYP inhibition assay

CYP inhibition was performed with the use of recombinant enzymes CYP1A2, CYP2B6, CYP2C19, CYP2D6 and CYP3A4 obtained from BD Biosciences. Compounds for CYP inhibition testing were prepared as 10 mM stock solutions in DMSO. Isoform-specific substrates were incubated at 37 °C individually with P450 enzymes (Table 10) and a range of test compound concentrations (1.1, 3.3 and 10  $\mu$ M) in duplicates. Each isoform was tested separately with one reference compound, known positive control inhibitor. During preincubation, the 96-well black plates were scanned with a fluorescence plate reader in order to eliminate false results originating from autofluorescence of the test compounds. At the end of the incubation, product formation was monitored with fluorescence detection. A decrease in the formation of the metabolite compared to “no inhibition” control samples was used to calculate an  $IC_{50}$  value.

##### 4.4.5. In vivo PK

All animals were handled in strict accordance with good animal practice, and maintained according to the standards of pathogen-free conditions. Experiment was approved by the 1st Local Ethical Committee for Animal Research in Krakow, Poland [approval 197/2014]. The pharmacokinetic profile of compound **24** and **26** was assessed in 5-week-old female CD-1 mice (outbred colony, Charles River Laboratories) (3 animals per time point). Compounds were freshly dissolved in DMSO and then diluted in Captisol (Ligand) for administration with a volume of 10  $\mu$ l per 1g of body weight via the oral (p.o.; 5 mg/kg) or i.v. (2 mg/kg) route. Animals were sacrificed

**Table 10**  
Experimental conditions summary - cytochrome P450 IC<sub>50</sub> inhibition determination assay.

P450 isoform	Positive control highest concentration (μM)	Substrate concentration (μM)	Enzyme concentration (nM)	Incubation length (min)
<b>CYP1A2</b>	Furafylline 5	CEC 5	5	15
<b>CYP2B6</b>	Tranylcypromine 50	EFC 2.5	10	30
<b>CYP2C19</b>	Tranylcypromiine 10	CEC 25	10	30
<b>CYP2D6</b>	Quinidine 0.05	AMMC 1.5	15	30
<b>CYP3A4</b>	Ketoconazole 0.05	BFC 50	5	30

at 8 time points (5, 15, and 30 min and 1, 2, 4, 7, and 24 h) and blood samples harvested. Plasma samples were collected and stored at -80 °C for further analysis.

**4.4.5.1. Sample analysis.** Investigated compounds **24** and **26** were dissolved in DMSO in order to obtain 10 mM stock solutions. Solutions were used for calibration curve preparation (16 calibration points, dilution factor x2, 10 000 ng/ml → 0.2 ng/ml, including blank sample). A solution of compounds **24** and **26** in acetonitrile and serial dilutions were prepared. The calibration curve was prepared in blank plasma. 5 μl of each solution was added to 45 μl of blank plasma. 200 μl of cold acetonitrile was added to each well. Next, plasma samples with the compounds were prepared in the same manner as samples. 50 μl of each plasma sample was dispensed into appropriate wells of 96-deep well plate. 200 μl of cold acetonitrile was added to each well. Plate was centrifuged (2000×g at 4 °C for 20 min). 170 μl of supernatant was transferred into a 96-well plate. The plate was covered with a silicone plate mat. Samples were analyzed using LC-MS technique. Concentrations of compounds in plasma samples were calculated using a calibration curve prepared in blank mice plasma.

**4.4.5.2. Conditions of the liquid chromatography-mass spectrometry.** Dionex Ultimate 3000 RS HPLC of the Thermo Scientific and Thermo Scientific TSQ Quantiva model was used. The conditions were: Column HPLC Ascentis Express C18 (5 cm × 2.1 mm, 2.7 μm), the injection volume was 1 μl. An acetonitrile gradient was used with 0.1% formic acid with 0.1% of formic acid in water at a constant flowrate of 0.6 ml/min. The programming was the following: 0–0.1 min 5% of ACN, 0.1–2.0 min increase of 5–98%, 2.0–3.0 min remaining at 98% of ACN, 3.0–3.2 min decrease of 98–5% and 3.2–4.0 min 5% of ACN. Mass spectrometry was conducted in tandem with the triple stage quadrupole analyzer in SRM mode, equipped with an heated-electrospray ionization source (H-ESI) in positive mode. The conditions of the main parameters were: spray voltage of 3.5 kV, sheath gas flow (Arb) of 52, auxiliary gas flow (Arb) of 16, sweep gas flow (Arb) of 2, drying gas temperature of 420C, ion transfer tube temperature of 356C and positive polarity. [Table 11](#) shows the values of precursor ions (*m/z*), retention time (RT) and collision energy (V) optimized for the identification of each compound.

**Table 11**  
Mass spectrometer SRM mode parameters.

Compound	Molecular weight (g/mol)	Precursor <i>m/z</i> (Th)	Product <i>m/z</i> (Th)	Collision energy (V)	RT (min)
<b>24</b>	334.35	335.16	198.04	33.056	1.97
<b>24</b>	334.35	335.16	226.06	25.522	1.97
<b>26</b>	350.81	351.15	198.06	34.169	2.08
<b>26</b>	350.81	351.15	226.06	26.008	2.08

## 5. Endotoxin survival studies

16 weeks old C57BL/6 male mice, were housed in the Department of Genetics, at the Maria Skłodowska-Curie National Research Institute of Oncology. Experimental protocol was approved by the 2nd Local Ethical Committee for Animal Research in Warsaw, Poland [approval WAW2/47/2017]. All animals will be checked for any ongoing inflammation (rash, fever, pain, swelling) prior to the experiment. The procedure was conducted by an experienced veterinarian and animals are monitored following 2 h post-LPS every 30 min and then every 6 h. Mice were injected intraperitoneally with lethal dose of endotoxin solution in saline (lipopolysaccharide [LPS]; L9143-02; Sigma), 20 mg/kg [44], or with saline alone and monitored every 2 h post injection for 6 h followed by every 6 h for remaining days. Compounds **24** and **26** were reconstituted in DMSO 3% + DMA 10% + Captisol 20% formulation and administrated *per os*, at the final concentration of 25 mg/kg and 75 mg/kg (survival experiment) or 50 mg/kg and 75 mg/kg, for compound **26** and **24**, respectively, an hour prior to LPS injection and then with BID regimen every 12 h. The control group was administrated with the DMSO/DMA/Captisol formulation. To prevent dehydration animals were given subcutaneous fluids (sterile normal saline) and had constant access to water. Mice were euthanized by isoflurane overdose and spinal cord dislocation when they became moribund according to the Murine Sepsis Score [45]. Necropsy and organs examination was performed on each mouse according to previous recommendations [46]. Tissues were flash frozen in liquid nitrogen while blood collected for serum for downstream analyses.

## 6. Statistical analysis

Statistical analysis was performed using the GraphPad Prism 6 software. The survival rates were tested with the log-rank Mantel-Cox test while the serum cytokines levels with Mann-Whitney *U* test. The significance of mean comparison is annotated as follows: ns, non-significant ( $p \geq 0.05$ ), \* $p < 0.05$ . Results were considered significant when  $p$ -value  $< 0.05$ .

## Funding sources

This work was supported by National Center for Research and

Development, Poland, INNOTECH Program (INNOTECH-K1/HI1/16/157483/NCBR/12) and the Polish National Science Center, Poland [2014/14/M/NZ5/00462 to MMikula].

### Declaration of competing interest

The authors declare that they have no known competing financial interests or personal relationships that could have appeared to influence the work reported in this paper.

### Appendix A. Supplementary data

Supplementary data to this article can be found online at <https://doi.org/10.1016/j.ejmech.2020.113057>.

### References

- [1] A. Dreas, M. Mikulski, M. Milik, C.-H. Fabritius, K. Brzózka, T. Rzymiski, Mitogen-activated protein kinase (MAPK) interacting kinases 1 and 2 (MNK1 and MNK2) as targets for cancer therapy: recent progress in the development of MNK inhibitors, *Curr. Med. Chem.* 24 (2017) 3025–3053.
- [2] S. Joshi, L.C. Platanius, Mnk kinase pathway: cellular functions and biological outcomes, *World J. Biol. Chem.* 5 (2014) 321–333.
- [3] Y. Zhan, J. Guo, W. Yang, C. Goncalves, T. Rzymiski, A. Dreas, et al., MNK1/2 inhibition limits oncogenicity and metastasis of KIT-mutant melanoma, *J. Clin. Invest.* 127 (2017) 4179–4192.
- [4] E.M. Kosciuczuk, D. Saleiro, L.C. Platanius, Dual targeting of eIF4E by blocking MNK and mTOR pathways in leukemia, *Cytokine* 89 (2017) 116–121.
- [5] N. Siddiqui, N. Sonenberg, Signalling to eIF4E in cancer, *Biochem. Soc. Trans.* 43 (2015) 763–772.
- [6] X. Yuan, H. Wu, H. Bu, P. Zheng, J. Zhou, H. Zhang, Design, synthesis and biological evaluation of pyridone-aminal derivatives as MNK1/2 inhibitors, *Bioorg. Med. Chem.* 27 (2019) 1211–1225.
- [7] S.H. Reich, P.A. Sprengeler, G.G. Chiang, J.R. Appleman, J. Chen, J. Clarine, et al., Structure-based design of pyridone-aminal eFT508 targeting dysregulated translation by selective mitogen-activated protein kinase interacting kinases 1 and 2 (MNK1/2) inhibition, *J. Med. Chem.* 61 (2018) 3516–3540.
- [8] S. Santag, F. Siegel, A.M. Wengner, C. Lange, U. Bömer, K. Eis, et al., BAY 1143269, a novel MNK1 inhibitor, targets oncogenic protein expression and shows potent anti-tumor activity, *Canc. Lett.* 390 (2017) 21–29.
- [9] A.J. Waskiewicz, A. Flynn, C.G. Proud, J.A. Cooper, Mitogen-activated protein kinases activate the serine/threonine kinases Mnk1 and Mnk2, *EMBO J.* 16 (1997) 1909–1920.
- [10] A. O'Loughlin, V.M. González, D. Piñeiro, M.I. Pérez-Morgado, M. Salinas, M.E. Martín, Identification and molecular characterization of Mnk1b, a splice variant of human MAP kinase-interacting kinase Mnk1, *Exp. Cell Res.* 299 (2004) 343–355.
- [11] K. Slentz-Kesler, J.T. Moore, M. Lombard, J. Zhang, R. Hollingsworth, M.P. Weiner, Identification of the human Mnk2 gene (MKNK2) through protein interaction with estrogen receptor beta, *Genomics* 69 (2000) 63–71.
- [12] G.C. Scheper, J.L. Parra, M. Wilson, B. Van Kollenburg, A.C.O. Vertegaal, Z.-G. Han, et al., The N and C termini of the splice variants of the human mitogen-activated protein kinase-interacting kinase Mnk2 determine activity and localization, *Mol. Cell Biol.* 23 (2003) 5692–5705.
- [13] J.L. Parra, M. Buxadé, C.G. Proud, Features of the catalytic domains and C termini of the MAPK signal-integrating kinases Mnk1 and Mnk2 determine their differing activities and regulatory properties, *J. Biol. Chem.* 280 (2005) 37623–37633.
- [14] R. Fukunaga, T. Hunter, MNK1, a new MAP kinase-activated protein kinase, isolated by a novel expression screening method for identifying protein kinase substrates, *EMBO J.* 16 (1997) 1921–1933.
- [15] A.J. Waskiewicz, J.C. Johnson, B. Penn, M. Mahalingam, S.R. Kimball, J.A. Cooper, Phosphorylation of the cap-binding protein eukaryotic translation initiation factor 4E by protein kinase Mnk1 in vivo, *Mol. Cell Biol.* 19 (1999) 1871–1880.
- [16] J.-L. Parra-Palau, G.C. Scheper, M.L. Wilson, C.G. Proud, Features in the N and C termini of the MAPK-interacting kinase Mnk1 mediate its nucleocytoplasmic shuttling, *J. Biol. Chem.* 278 (2003) 44197–44204.
- [17] T. Ueda, R. Watanabe-Fukunaga, H. Fukuyama, S. Nagata, R. Fukunaga, Mnk2 and Mnk1 are essential for constitutive and inducible phosphorylation of eukaryotic initiation factor 4E but not for cell growth or development, *Mol. Cell Biol.* 24 (2004) 6539–6549.
- [18] Y. Mamane, E. Petroulakis, L. Rong, K. Yoshida, L.W. Ler, N. Sonenberg, eIF4E—from translation to transformation, *Oncogene* 23 (2004) 3172–3179.
- [19] R.M. Rowlett, C.A. Chrestensen, M. Nyce, M.G. Harp, J.W. Pelo, F. Cominelli, et al., MNK kinases regulate multiple TLR pathways and innate proinflammatory cytokines in macrophages, *Am. J. Physiol. Gastrointest. Liver Physiol.* 294 (2008) G452–G459.
- [20] S. Joshi, L.C. Platanius, Mnk kinases in cytokine signaling and regulation of cytokine responses, *Biomol. Concepts* 3 (2012) 127–139.
- [21] S. Lv, M. Han, R. Yi, S. Kwon, C. Dai, R. Wang, Anti-TNF- $\alpha$  therapy for patients with sepsis: a systematic meta-analysis, *Int. J. Clin. Pract.* 68 (2014) 520–528.
- [22] C.E. Spooner, N.P. Markowitz, L.D. Saravolatz, The role of tumor necrosis factor in sepsis, *Clin. Immunol. Immunopathol.* 62 (1992) S11–S17.
- [23] R. Plevin, R. Callcut, Update in sepsis guidelines: what is really new? *Trauma Surg. Acute Care Open* 2 (2017), e000088.
- [24] S. Jain, Sepsis: an update on current practices in diagnosis and management, *Am. J. Med. Sci.* 356 (2018) 277–286.
- [25] H.K. de Jong, T. van der Poll, W.J. Wiersinga, The systemic pro-inflammatory response in sepsis, *J. Innate Immun.* 2 (2010) 422–430.
- [26] B.G. Chousterman, F.K. Swirski, G.F. Weber, Cytokine storm and sepsis disease pathogenesis, *Semin. Immunopathol.* 39 (2017) 517–528.
- [27] S.M. Opal, T. van der Poll, Endothelial barrier dysfunction in septic shock, *J. Intern. Med.* 277 (2015) 277–293.
- [28] P. Seidel, Q. Sun, L. Costa, D. Lardinois, M. Tamm, M. Roth, The MNK-1/eIF4E pathway as a new therapeutic pathway to target inflammation and remodeling in asthma, *Cell. Signal.* 28 (2016) 1555–1562.
- [29] J. Hou, F. Lam, C. Proud, S. Wang, Targeting Mnk for cancer therapy, *Oncotarget* 3 (2012) 118–131.
- [30] X.-B. Huang, C.-M. Yang, Q.-M. Han, X.-J. Ye, W. Lei, W.-B. Qian, MNK1 inhibitor CGP57380 overcomes mTOR inhibitor-induced activation of eIF4E: the mechanism of synergic killing of human T-ALL cells, *Acta Pharmacol. Sin.* 39 (2018) 1894–1901.
- [31] Q. Wen, W. Wang, J. Luo, S. Chu, L. Chen, L. Xu, et al., CGP57380 enhances efficacy of RAD001 in non-small cell lung cancer through abrogating mTOR inhibition-induced phosphorylation of eIF4E and activating mitochondrial apoptotic pathway, *Oncotarget* 7 (2016) 27787–27801.
- [32] J.K. Altman, A. Szilard, B.W. Konicek, P.W. Iversen, B. Kroczyńska, H. Glaser, et al., Inhibition of Mnk kinase activity by cercosporamide and suppressive effects on acute myeloid leukemia precursors, *Blood* 121 (2013) 3675–3681.
- [33] U. Knauf, C. Tschoop, H. Gram, Negative regulation of protein translation by mitogen-activated protein kinase-interacting kinases 1 and 2, *Mol. Cell Biol.* 21 (2001) 5500–5511.
- [34] H. Yang, L.R. Chennamaneni, M.W.T. Ho, S.H. Ang, E.S.W. Tan, D.A. Jeyaraj, et al., Optimization of selective mitogen-activated protein kinase interacting kinases 1 and 2 inhibitors for the treatment of blast crisis leukemia, *J. Med. Chem.* 61 (2018) 4348–4369.
- [35] H.M. Berman, J. Westbrook, Z. Feng, G. Gilliland, T.N. Bhat, H. Weissig, et al., The Protein Data Bank, *Nucleic Acids Res.* 28 (2000) 235–242.
- [36] Schrödinger. Schrödinger Release 2018-1, LLC, New York, 2016.
- [37] R. Jauch, M.-K. Cho, S. Jäkel, C. Netter, K. Schreiter, B. Aicher, et al., Mitogen-activated protein kinases interacting kinases are autoinhibited by a reprogrammed activation segment, *EMBO J.* 25 (2006) 4020–4032.
- [38] J.Y. Ramphal, B.O. Buckman, K. Emayan, J.B. Nicholas, S.D. Seiwert, Antifibrotic pyridinones [Internet]. 2015 [cited 2019 Jun 7]. Available from: <https://patents.google.com/patent/WO2015153683A1/en>.
- [39] R. Benarous, F. Chevreuil, B. Ledoussal, S. Chasset, F.L. Strat, Inhibitors of viral replication, their process of preparation and their therapeutic uses [Internet]. 2014 [cited 2019 Jun 7]. Available from: <https://patents.google.com/patent/WO2014057103A1/en?qoq=WO2014057103A1>.
- [40] D. Demong, T.J. Greshock, R.K. Chang, X. Dai, H. Liu, J.A. Mccauley, et al., Compounds inhibiting leucine-rich repeat kinase enzyme activity [Internet]. 2015 [cited 2019 Jun 7]. Available from: <https://patents.google.com/patent/WO2015026683A1/en?qoq=WO2015026683A1>.
- [41] H. Zhang, P. Chen, G. Liu, Palladium-catalyzed oxidative aryalkylation of unactivated alkenes: dual C–H bond cleavage of anilines and acetonitrile, *Synlett* 23 (2012) 2749–2752.
- [42] K. Andersson, R. Sundler, Posttranscriptional regulation of TNF $\alpha$  expression via eukaryotic initiation factor 4E (eIF4E) phosphorylation in mouse macrophages, *Cytokine* 33 (2006) 52–57.
- [43] C.F. Fortin, T.Z. Mayer, A. Cloutier, P.P. McDonald, Translational control of human neutrophil responses by MNK1, *J. Leukoc. Biol.* 94 (2013) 693–703.
- [44] M.E. Starr, J. Ueda, H. Takahashi, H. Weiler, C.T. Esmon, B.M. Evers, et al., Age-dependent vulnerability to endotoxemia is associated with reduction of anticoagulant factors activated protein C and thrombomodulin, *Blood* 115 (2010) 4886–4893.
- [45] B. Shrum, R.V. Anantha, S.X. Xu, M. Donnelly, S.M. Haeryfar, J.K. McCormick, et al., A robust scoring system to evaluate sepsis severity in an animal model, *BMC Res. Notes* 7 (2014) 233.
- [46] D.B. Feldman, J.C. Seely, *Necropsy Guide: Rodents and the Rabbit*, CRC Press, Boca Raton, FL, 1988. Available from: <https://www.taylorfrancis.com/books/9781482216073>.